

Studies of RR Lyrae Variables in Binary Systems. I.: Evidence of a Trimodal Companion Mass Distribution

GERGELY HAJDU,¹ GRZEGORZ PIETRZYŃSKI,¹ JOHANNA JURCSIK,² MÁRCIO CATELAN,^{3,4} PAULINA KARCZMAREK,⁵
BOGUMIŁ PILECKI,¹ IGOR SOSZYŃSKI,⁶ ANDRZEJ UDALSKI,⁶ AND IAN B. THOMPSON⁷

¹*Nicolaus Copernicus Astronomical Center, Polish Academy of Sciences, Bartycka 18, Warsaw, 00-716, Poland*

²*Konkoly Observatory, Research Centre for Astronomy and Earth Sciences, Eötvös Loránd Research Network (ELKH), Konkoly Thege Miklós út 15-17., Budapest, H-1121, Hungary*

³*Pontificia Universidad Católica de Chile, Facultad de Física, Instituto de Astrofísica, Av. Vicuña Mackenna 4860, 7820436 Macul, Santiago, Chile*

⁴*Millennium Institute of Astrophysics, Nuncio Monseñor Sotero Sanz 100, Of. 104, Providencia, Santiago, Chile*

⁵*Universidad de Concepción, Departamento de Astronomía, Casilla 160-C, Concepción, Chile*

⁶*Astronomical Observatory, University of Warsaw, Aleje Ujazdowskie 4, Warsaw, 00-478, Poland*

⁷*The Observatories of the Carnegie Institution for Science, 813 Santa Barbara Street, Pasadena, CA 91101, USA*

(Received April 20, 2021; Revised May 5, 2021; Accepted May 7, 2021)

ABSTRACT

We present 87 candidates for RR Lyrae variable stars in binary systems, based on our new search using the light-travel time effect (LTTE) and observed – calculated ($O - C$) diagrams in the Galactic bulge time-series photometry of the Optical Gravitational Lensing Experiment. Out of these, 61 are new candidates, while 26 have been announced previously. Furthermore, 12 stars considered as binary candidates in earlier works are discarded from the list, either because they were found to have $O - C$ diagrams incompatible with the LTTE or because their long-term periodicity is definitely caused by the Blazhko effect.

This sample of RR Lyrae binary candidates allows us to draw the first firm conclusions about the population of such objects: no candidate has an orbital period below 1000 days, while their occurrence rate steadily increases with increasing period, and peaks between 3000 and 4000 days; however, the decrease in the number of stars toward even longer periods is probably the result of observational biases. The eccentricities show a very significant concentration between 0.25 and 0.3, with a quarter of candidates found in this single bin, overlaid on an otherwise flat distribution between 0.05 and 0.6. Only six stars have higher inferred eccentricities above 0.6. Lastly, the distribution of the mass functions is highly peculiar, exhibiting strong trimodality. We interpret these modes as the presence of three distinct groups of companions, with typical inferred masses of ~ 0.6 , ~ 0.2 , and $\sim 0.067 M_{\odot}$, which can be associated with populations of white dwarf and main sequence, red dwarf, and brown dwarf companions, respectively.

Keywords: RR Lyrae variable stars(1410) — Binary stars(154) — Time series analysis(1916) — Astronomy data analysis(1858) — Stellar masses(1614) — Stellar astronomy(1583)

1. INTRODUCTION

After more than 100 years of continuous study, RR Lyrae variables (hereafter RRLs) remain at the forefront of astrophysics, including their use as distance indicators toward old stellar populations (e.g., Karczmarek et al. 2017; Beaton et al. 2018), the study of the 3D structure of old stellar populations in nearby galaxies (e.g., Jacyszyn-Dobrzeńska et al. 2017; Hernitschek et al. 2018; Ferguson & Strigari 2020),

the behavior of interstellar extinction (e.g., Saha et al. 2019), and even as probes of their metallicity distributions (e.g., Martínez-Vázquez et al. 2016; Vivas et al. 2020).

Despite our extensive knowledge of these variables, and the large number of members (well over 100,000) discovered in the Milky Way and its satellite galaxies by sky surveys such as the Optical Gravitational Lensing Experiment (OGLE; Magellanic System: Soszyński et al. 2016; Milky Way bulge and disk: Soszyński et al. 2019), the variability survey of the *Gaia* satellite (Clementini et al. 2019), the Catalina Sky Survey (Torrealba et al. 2015), Pan-STARRS (Sesar et al. 2017), and the Vista Variables in the Vía Láctea (Dékány & Grebel 2020) among others, the arguably most

important stellar property, the stellar mass, has never been measured directly even for a single member of this class. As the most straightforward way to measure stellar masses is by characterizing the orbits of members of binary systems, searches for binary RRLs have been carried out, but until very recently, only the variable TU UMa had been demonstrated to reside in one with high certainty (Wade et al. 1999; Liška et al. 2016a). The very long (~ 23 yr) orbital period, combined with no detection of light from the companion, hinders the complete characterization of this system.

Sky surveys have found very few candidates for RRLs in eclipsing binary systems, with spectroscopic follow-up confirming them as either blends (Prša et al. 2008) or, in the case of OGLE-BLG-RRLYR-02792, an entirely new kind of variable star, a so-called binary evolution pulsator (BEP; Pietrzyński et al. 2012; Smolec et al. 2013). This is not an entirely unexpected result: in a close binary system Roche-lobe overflow would happen while the star traverses the red giant branch. This would result in too much mass loss before it evolves onto the horizontal branch (HB) to settle inside the main instability strip, resulting in a blue HB star instead (see, e.g., Vos et al. 2020, as well as references therein). Therefore, bona fide binary RRLs are necessarily located in wide binary systems (with orbital periods longer than around 1000 days), greatly diminishing the probability of finding one in an eclipsing system.

The most widely utilized method in the search for RRL binaries uses the light-travel time effect (LTTE; Irwin 1952, 1959), the modulation of the light curves induced by the changing distance between the observer and the pulsating component in a binary system due to its motion around the center of mass. Most commonly, these changes are quantified using the so-called observed – calculated ($O - C$) diagrams (Sterken 2005), which are constructed using the timings of specific parts of the light curve of the variable in question (e.g., maxima of the light curve, or the middle of the rising branch for pulsating variables; light-curve minima for eclipsing variables) and the period of the variable. This diagram is then analyzed looking for the characteristic shape expected of the LTTE. This method was used in the context of the high-precision Kepler space telescope observations (Li & Qian 2014; Guggenberger & Steixner 2015; Sódor et al. 2017), as well as for field RRL variables that can have $O - C$ diagrams spanning over 100 years (Derekas et al. 2004; Liška et al. 2016b; Li et al. 2018a,b) to identify a number of binary candidates. However, it should be noted that in the only published case where radial velocity observations were available to revise the claimed binarity, this possibility has been conclusively discarded (Z CVn; Skarka et al. 2018).

An alternative way to construct $O - C$ diagrams is by following the proposal of Hertzprung (1919), and measuring the phase shift of the whole light curve using a template.

This technique is particularly well suited for use on data obtained by wide-field variability surveys, where the random nature of the time sampling usually results in well-covered light curves. For such data sets, measuring the times of individual maxima may actually be impossible, depending on the sparsity of the sampling. However, a significant drawback of this method is that care must be taken both during the construction of the light-curve template and during the definition of the sections of the light curves, because choices made for these crucial points can have a drastic effect on the quality of the $O - C$ diagram. Nevertheless, we have utilized this method in our initial search for RRL binary candidates (Hajdu et al. 2015) with the OGLE survey light curves (Udalski et al. 2015a) of RRLs toward the Galactic bulge. The aforementioned drawbacks were reduced mostly by resorting to an iterative process for the construction of the template light curves, where we have corrected the light curves for an initial binary $O - C$ solution, and refitted the template to these corrected data. These new templates, which resembled the intrinsic light-curve shape of their respective stars much better (when compared to the initial ones), allowed the derivation of much more accurate $O - C$ points. The binary RRL candidate sample was further extended by Prudil et al. (2019), who used similar procedures to those described in Hajdu et al. (2015).

It is worth mentioning that traditional $O - C$ diagrams are not the only way of characterizing the LTTE: phase-modulated light curves in Fourier space exhibit characteristic structures that can also be modeled, allowing the determination of orbital parameters with high accuracy (Shibahashi & Kurtz 2012; Shibahashi et al. 2015). This technique has been tried for RRL stars already (Shibahashi 2017), although it might not be entirely suited for the study of this particular class of variables: generally the available data span only a few times the length of the supposed orbital periods, resulting in wide peaks for the characteristic frequencies in Fourier space. This, as well as the intrinsic, slow change of the period of pulsation, limits the accuracy of the technique. Nevertheless, it is a very valuable tool for shorter-period variables (e.g., δ Scuti, SX Phe, or various classes of pulsating white dwarfs), allowing us to study their general binarity parameters (Murphy et al. 2018), and sensitive enough to discover exoplanets (Murphy et al. 2016). Another method, forward modeling of modulated light curves, has been proposed as an alternative characterization of the LTTE very recently (Hey et al. 2020). This technique holds a lot of promise, and its applicability should be explored in the context of RRL stars in the future.

Regardless of the exact method, the information learned from the LTTE for a well characterized variable is the same as that provided by radial velocity observations of a single-lined spectroscopic binary (SB1): the projected orbit of the variable is characterized, but no information is provided on

either of the inclination of the system or on the mass ratio of its components. For this reason, additional constraints (radial velocity follow-up; astrometry; theoretical considerations) are a must for learning more about these systems.

Besides the LTTE, radial velocity observations can also be used to discover RRLs in binary systems, similarly to other types of stars. However, this is significantly more difficult for RRL variables, because their rapid, large-amplitude pulsations must be disentangled from the expected long-term, small-amplitude binary signal. There is one project currently attempting this (Guggenberger et al. 2016); however, it has not yet resulted in the announcement of new RRL binary candidates.

The detection of binary RRLs through their astrometric motion (Kervella et al. 2019a), as well as identification of their resolved companions by common proper motions (Kervella et al. 2019b) and high-resolution imaging techniques (Salinas et al. 2020), has been attempted only very recently. While these techniques are very promising, full characterization of a binary orbit might still be unattainable if the companion is very faint (e.g., a stellar remnant) or if the orbital period is too long for follow-up observations.

Finally, RRL variables with chemical abundance anomalies, such as carbon enhancement (Hansen et al. 2011; Kennedy et al. 2014) and even overabundance of neutron-capture elements (TY Gru; Preston et al. 2006) might be explained by pollution of the stellar atmosphere by earlier mass transfer from an asymptotic giant branch (AGB) companion (Stanciliffe et al. 2013). Nevertheless, none of these stars have been confirmed to reside in a binary system so far.

In this new series of papers, we are undertaking a systematic study of binary RRL variables, and in this initial paper we are specifically searching for new candidates in the OGLE Galactic bulge light curves. As some of these data have been searched before both by us (Hajdu et al. 2015, 2018) and by an independent group (Prudil et al. 2019), we also revise the list of prospective RRL binaries announced so far. Our final candidate list now has enough variables to draw meaningful conclusions about the companion population of RRLs in binary systems, even if some of them will likely turn out to be false candidates in the future.

2. DATA AND THE SEARCH FOR BINARY CANDIDATES

During this new search, we have used an updated catalog of the OGLE RRL variables toward the Galactic bulge, published by Soszyński et al. (2014), with the *I*-band light curves including observations until the 2017 observing season. All OGLE observations were obtained with the 1.3 m Warsaw telescope at Las Campanas observatory (Udalski et al. 2015a). Although many more RRLs have been published by the OGLE project in the Galactic bulge and disk

owing to the OGLE Galaxy Variability Survey (Soszyński et al. 2019), their light curves are generally too short to conduct a search for binary signals that are multiple years long. As in our previous work (Hajdu et al. 2015), here we consider only fundamental-mode RRL variables (RRab subtype).

2.1. Construction of the initial $O - C$ diagrams

Our initial $O - C$ diagrams were constructed using similar, but slightly modified procedures to those in Hajdu et al. (2015), expanding upon the original method of Hertzprung (1919). It is important to note that stars observed during both the OGLE-III and IV phases of the OGLE project have effectively two independent, non-overlapping *I*-band light curves. Although these light curves were derived using similar procedures, one must exercise caution when attempting to combine them, because they use different cameras and filters (see Udalski et al. 2015a for an overview), therefore can have different magnitude zero-points. The OGLE project uses image subtraction combined with zero points derived using point-spread function photometry. While image subtraction is expected to produce consistent results on the *intensity scale*, even a small error in the zero point for either the OGLE-III or IV (or both) part(s) of the light curve will result in different average magnitudes. Furthermore, the brighter of the two parts will have diminished pulsation amplitude on the *magnitude scale* when compared to the fainter section. Therefore, as a first step, for each star we have transformed both the OGLE-III and IV photometries to an arbitrary intensity scale. Both sections of the light curve were then fitted independently with a fifth-order truncated Fourier series, and the OGLE-III photometry was shifted to the mean level of the OGLE-IV observations, before finally transforming it back to the magnitude scale. We note that in Hajdu et al. (2015) the difference between the OGLE-III and IV photometry was only corrected for by a simple shift in magnitude.

During the second step, the homogenized (if both OGLE-III and OGLE-IV data were available) light curves were folded using their periods given by Soszyński et al. (2014), and fitted with a fifth-order truncated Fourier series using ordinary least-squares (OLS) regression to serve as the light-curve template. Then, the light curve was divided first into observing seasons, and each season was further divided into two segments if more than 40 light-curve points were available (in Hajdu et al. 2015, this was done if within a season the baseline of observations exceeded 160 days, but sometimes this resulted in sections having very few points, hence the change). The $O - C$ points were then derived as the phase shift that minimized the scatter between the light-curve template and the points in each of the individual segments.

In total, 27,480 $O - C$ diagrams were constructed in this way for RRab variables (with the last one being OGLE-BLG-RRLYR-39119; hereafter, every OGLE bulge RRL star will

be referred to only by its numerical ID), and all of them were inspected, simultaneously with their light curves (both original and folded). The average and median numbers of data points were 2483 and 766, while the average and median time baselines were 10.5 and 7.4 yr, respectively. As mentioned in Section 1, the exact way in which the template light curve is constructed can have a big impact on the individual $O - C$ measurements, possibly introducing biases that could hinder the recognition of the LTTE. In order to compensate for this, we have selected all candidates with $O - C$ shapes even vaguely resembling the expected LTTE for further analysis, resulting in a list of ~ 400 RRL variables. Contrary to the restrictive approach employed in Hajdu et al. (2015), we have not discarded stars showing the Blazhko effect (Blažko 1907; see also Smolec 2016 for a recent review and additional references), and also included all previously announced binary candidates from Hajdu et al. (2015, 2018) and Prudil et al. (2019), as well.

2.2. Analysis of the Light-travel Time Effect

The effect of the LTTE on the $O - C$ diagrams can be modeled by its characteristic shape, following Irwin (1952, 1959). Throughout this work, we have adopted the LTTE shape as

$$z(t) = a_1 \sin i \frac{1 - e^2}{1 + e \cos(\nu)} \sin(\nu + \omega), \quad (1)$$

where $z(t)$ is the time-dependent distance between the observer and the variable component of the binary, $a_1 \sin i$ is the projected semimajor axis of the RRL, e is the eccentricity, ω is the argument of the periastron, and ν is the true anomaly. We recall that the latter quantity can be calculated for any point in time through

$$\cos \nu = \frac{\cos E - e}{1 - e \cos E}, \quad (2)$$

where the eccentric anomaly E is connected to the mean anomaly M by

$$M = E - e \sin E = \frac{2\pi}{P_{\text{orb}}} (t - T_0), \quad (3)$$

which itself is a linear function of time, depending on the orbital period P_{orb} , the time of periastron passage T_0 , and the time of observations t .

Unfortunately, the LTTE interpretation of the $O - C$ diagrams is complicated by the fact that changes in the variability period accumulate over time. When this change is approximately linear, as is expected from evolutionary changes on human time scales for RRL stars, this causes an additional, parabolic shape to be present in the $O - C$ diagram. We can extend Equation 1 to model it as

$$(O - C)(t) = z(t) + c_0 + c_1 \cdot t + c_2 \cdot t^2, \quad (4)$$

where c_1 is the fractional difference between the period used to construct the $O - C$ diagram and the pulsational period at $t = 0$, while c_2 is related to the linear period-change rate (Sterken 2005) as:

$$\beta = c_2 \cdot 2 \cdot P, \quad (5)$$

where P is the pulsational period of the RRL in question adopted for the construction of its $O - C$ diagram.¹ The period-change rate β is usually expressed in units of day Myr^{-1} for RRL variables. The (absolute) value of this parameter is generally smaller than 0.5 day Myr^{-1} for most regular RRLs (see, e.g., Jurcsik et al. 2001; Szeidl et al. 2011; Jurcsik et al. 2012a).

For the initial analysis of the ~ 400 stars selected in Section 2.1, we used a very similar iterative procedure to that outlined in Hajdu et al. (2015), but also supplemented the light curves with OGLE observations taken in 2018 and 2019.² The initial $O - C$ diagrams were prepared for this data set as described in Section 2.1. Then, the $O - C$ points were fit with Equation 4 to model the shape of the $O - C$ diagram expected from the combination of the LTTE and a linear period change of the pulsational period of the RRL variables. The fit was then subtracted from the timings of the individual I -band observations, resulting in modified light curves mostly devoid of the effect of both the LTTE and the linear period change.

The modified light curve was used to construct an improved template, fit with a higher-order Fourier series, which follows the real light-curve shape much better, resulting in improved $O - C$ estimates when using them to redetermine their values. Furthermore, the uncertainties of these new $O - C$ points were also estimated using bootstrapping, by drawing 500 new samples for each of the light-curve segments (for N points in a segment we drew N points with replacement). For each of the segments, the $O - C$ values of these 500 samples were also determined, and their standard deviations with respect to the non-bootstrapped estimates were adopted as their uncertainties.

This procedure was repeated multiple times for each of the variables, while simultaneously varying the assumed pulsa-

¹ It should be noted that this formula is different from that presented by Sterken (2005), where the variability period is in the denominator. The reason for this is the choice of the independent variable: in our case it is time t , while Sterken (2005) considers the epoch number E (not to be confused with the eccentric anomaly in Eqs. 2 and 3) as the independent variable.

² The extended light curves will be part of newer editions of the OGLE Catalog of Variable Stars. In the meantime they can be acquired from the OGLE team upon request.

tional period and the orders of the Fourier harmonics applied in each step of the iterations. At this point, stars were removed from the list for a variety of reasons. Some of these variables displayed clear (albeit sometimes tiny, ~ 0.01 mag) amplitude modulation with the same period as the supposed binary motion. Other stars deviated from the periodic $O - C$ behavior when the light curve was extended with the last two seasons of OGLE observations. In the case of many variables, mostly those with long purported binary periods and low amplitudes, it could not be decided from the available data whether a binary model was more favorable than a non-linear period-change behavior. Therefore, we have discarded them from further analysis. All in all, fewer than 100 variables remained after this step in our analysis.

2.3. Determination of the final parameters with MCMC

We continued analyzing the remaining candidates by further modifying the iterative procedure outlined in Section 2.2, changing it at three key points.

First, due to the short binary periods of some of the binary candidates, it became necessary to divide the light curves into smaller parts, because the expected $O - C$ values within a season could change more than their formal errors. Therefore, we adopted the following (default) scheme for dividing seasons into smaller segments: seasons with fewer than 9 points were not analyzed; those with 9 – 80 points were left as one segment; seasons with 81 – 120, 121 – 160, 161 – 240, and 241 or more points were divided into 2, 3, 4, and 5 segments, respectively. This division was only modified only in special cases (see Section 3).

Second, it was recognized that in cases of eccentricities with large errors (usually when the eccentricity itself is small or the $O - C$ diagram is noisy), the behavior of the argument of periastron can become erratic. This can be thought of as a result of the latter quantity losing its meaning at small eccentricities: when $e = 0$, the orbit is circular, and all points along it can be regarded as the periastron. Therefore, during the second iteration of the $O - C$ fitting procedure, instead of fitting the values of e and ω directly, we consider them as polar coordinates, and use their Cartesian equivalents $\sqrt{e} \sin \omega$ and $\sqrt{e} \cos \omega$ as free parameters. Then, the values of the original quantities can be recovered trivially as follows:

$$e' = (\sqrt{e} \sin \omega)^2 + (\sqrt{e} \cos \omega)^2, \quad (6)$$

$$\omega' = \arctan2(\sqrt{e} \sin \omega, \sqrt{e} \cos \omega), \quad (7)$$

which is similar to the conversion between parameters of the linear and nonlinear forms of harmonics of a Fourier series.

Finally, in the course of the second iteration of the procedure, for the estimation of the final binary parameters and their uncertainties, we have adopted a Bayesian formalism, leveraging the ensemble Markov Chain Monte Carlo (MCMC) capabilities of the EMCEE package (Foreman-Mackey et al. 2013). The calculations were done for all stars using the default sampler, implementing the affine-invariant ensemble stretch move presented by Goodman & Weare (2010). The current implementation of EMCEE supports alternative samplers, and even allows the use of a weighted mix of samplers during the MCMC procedure. We have conducted limited testing of these possibilities, but have found that in the case of our specific problem they generally have very similar or clearly inferior performance (for example, in terms of convergence and autocorrelation lengths) to the default one, and therefore we decided not to use them.

As our routines implementing the calculation of the $O - C$ shape (Eqs. 1 and 4) are somewhat inefficient due to the usage of the PYTHON programming language, we have experimented with the NUMBA (Lam et al. 2015) package to speed up critical parts of the computations. Using NUMBA with minimal changes to the code, a speedup of $\times 3 - 5$ was achieved during the MCMC fitting, allowing us to run longer chains and experiment with the fitting process more. In order to aid with the reproducibility of our results, the subroutines implementing the method described in this section are available on GitHub³, along with supporting Jupyter notebooks (Kluyver et al. 2016) showcasing their use for RRL stars.

3. THE ADOPTED LTTE SOLUTIONS OF THE BINARY RR LYRAE CANDIDATES

We have used the iterative $O - C$ procedure, with the MCMC implementation in the second iteration outlined in Section 2.3, to continue analyzing the stars remaining after the initial examination of prospective RRL binary candidates (Sect. 2.1). We choose to alter the process of dividing seasons into smaller segments for five variables: for 06992 and 08830 the data from 2001 were not used; for 09698 and 10142 the data from 2001 and 2002 were merged into one $O - C$ point to stabilize the LTTE solutions. Furthermore, due to the quick changes of the $O - C$ values (the combined result of a large period-change rate and a relatively short-period, large-amplitude LTTE component) for 20376, we decided to split all seasons into two sections, even though not all of them had more than 80 points.

³ https://github.com/gerhajdu/rrl_binaries.1

Table 1. Parameters of the binary RR Lyrae sample from the MCMC analysis

ID	P	P_{orb}	$a_1 \sin i$	e	ω	T_0	β	K_1	$f(m)$	$M_{S,\text{min.}}$	Quality
	(days)	(days)	(au)		(deg)	(days)	(day Myr $^{-1}$)	(km s $^{-1}$)	(M_{\odot})	(M_{\odot})	
02387	0.6722870	1947 \pm 14	1.562 \pm 0.084	0.370 \pm 0.092	121 \pm 16	8738 \pm 87	0.070 \pm 0.044	9.48 \pm 0.85	0.13521 \pm 0.02265	0.5935	Q1
02854	0.6002180	3478 \pm 20	2.328 \pm 0.079	0.454 \pm 0.052	128 \pm 6	8250 \pm 59	-0.061 \pm 0.027	8.20 \pm 0.45	0.13961 \pm 0.01428	0.6029	Q1
02950	0.4951840	2572 \pm 8	2.321 \pm 0.041	0.295 \pm 0.029	-159 \pm 5	6423 \pm 38	0.075 \pm 0.017	10.28 \pm 0.26	0.25230 \pm 0.01368	0.8151	Q1
04376	0.4910180	2909 \pm 19	0.755 \pm 0.022	0.423 \pm 0.059	-104 \pm 7	6505 \pm 54	0.071 \pm 0.005	3.13 \pm 0.18	0.00680 \pm 0.00064	0.1653	Q2
04628	0.5850070	2164 \pm 30	0.696 \pm 0.035	0.270 \pm 0.082	177 \pm 15	7279 \pm 91	0.064 \pm 0.024	3.66 \pm 0.28	0.00971 \pm 0.00161	0.1899	Q2
04837	0.5911800	4493 \pm 20	3.113 \pm 0.047	0.294 \pm 0.022	-47 \pm 4	3854 \pm 52	-0.110 \pm 0.018	7.89 \pm 0.15	0.19941 \pm 0.00917	0.7210	Q1
05089	0.4808195	2879 \pm 16	0.489 \pm 0.050	0.630 \pm 0.111	-67 \pm 7	6927 \pm 45	0.108 \pm 0.004	2.53 \pm 0.88	0.00194 \pm 0.00075	0.1032	Q2
05135	0.5191200	5795 \pm 85	3.888 \pm 0.070	0.180 \pm 0.013	51 \pm 3	3351 \pm 56	0.007 \pm 0.043	7.42 \pm 0.06	0.23352 \pm 0.00681	0.7826	Q2
05152	0.6201190	6645 \pm 328	3.642 \pm 0.194	0.352 \pm 0.029	-51 \pm 3	4075 \pm 53	0.494 \pm 0.066	6.37 \pm 0.12	0.14599 \pm 0.00954	0.6163	Q3
05239	0.5230260	3288 \pm 41	0.303 \pm 0.011	0.068 \pm 0.049	-127 \pm 64	5335 \pm 587	0.039 \pm 0.004	1.01 \pm 0.04	0.00034 \pm 0.00004	0.0556	Q2
05949	0.5007805	3285 \pm 15	2.109 \pm 0.018	0.326 \pm 0.015	-39 \pm 2	6073 \pm 21	-0.104 \pm 0.011	7.39 \pm 0.09	0.11596 \pm 0.00286	0.5510	Q2
06498	0.5894900	2803 \pm 3	2.493 \pm 0.010	0.136 \pm 0.008	-77 \pm 3	6537 \pm 25	-0.002 \pm 0.005	9.77 \pm 0.04	0.26296 \pm 0.00334	0.8332	Q1
06909	0.3731200	4204 \pm 47	1.443 \pm 0.055	0.302 \pm 0.067	136 \pm 13	6526 \pm 153	-0.179 \pm 0.011	3.93 \pm 0.20	0.02279 \pm 0.00265	0.2678	Q2
06981	0.6076795	4195 \pm 35	0.900 \pm 0.022	0.244 \pm 0.032	-162 \pm 7	5291 \pm 84	0.014 \pm 0.008	2.41 \pm 0.08	0.00554 \pm 0.00043	0.1528	Q1
06992	0.6075195	4897 \pm 233	0.442 \pm 0.037	0.252 \pm 0.080	156 \pm 18	4827 \pm 247	0.121 \pm 0.028	1.02 \pm 0.07	0.00048 \pm 0.00010	0.0627	Q3
07051	0.8680320	2238 \pm 24	1.023 \pm 0.038	0.284 \pm 0.072	-32 \pm 13	6856 \pm 83	0.469 \pm 0.024	5.21 \pm 0.26	0.02860 \pm 0.00317	0.2943	Q2
07079	0.5609450	6560 \pm 277	1.839 \pm 0.406	0.564 \pm 0.039	170 \pm 14	8114 \pm 115	0.137 \pm 0.230	3.69 \pm 0.76	0.02141 \pm 0.01509	0.2609	Q3
07275	0.4594780	5535 \pm 699	1.480 \pm 0.209	0.299 \pm 0.053	-12 \pm 5	6057 \pm 56	0.363 \pm 0.047	3.05 \pm 0.10	0.01412 \pm 0.00244	0.2203	Q3
07566	0.6768105	3517 \pm 8	1.745 \pm 0.022	0.508 \pm 0.013	177 \pm 1	5547 \pm 18	0.009 \pm 0.008	6.27 \pm 0.12	0.05736 \pm 0.00221	0.3979	Q1
07638	0.5553440	2285 \pm 9	1.251 \pm 0.027	0.216 \pm 0.043	-159 \pm 10	6535 \pm 63	0.067 \pm 0.015	6.11 \pm 0.17	0.05011 \pm 0.00325	0.3747	Q1
07640	0.5537705	1251 \pm 2	0.973 \pm 0.011	0.076 \pm 0.024	-54 \pm 20	8293 \pm 71	0.060 \pm 0.004	8.49 \pm 0.10	0.07854 \pm 0.00275	0.4588	Q1
07659	0.5052320	4922 \pm 131	0.350 \pm 0.011	0.076 \pm 0.047	-10 \pm 40	7970 \pm 572	-0.078 \pm 0.008	0.78 \pm 0.03	0.00024 \pm 0.00002	0.0487	Q3
07943	0.6043500	3847 \pm 16	1.414 \pm 0.018	0.174 \pm 0.024	-25 \pm 8	6679 \pm 84	0.031 \pm 0.007	4.06 \pm 0.06	0.02552 \pm 0.00101	0.2806	Q1
07995	0.4784280	6330 \pm 503	0.673 \pm 0.055	0.398 \pm 0.036	34 \pm 3	6373 \pm 42	0.079 \pm 0.008	1.26 \pm 0.02	0.00101 \pm 0.00009	0.0816	Q3
08185	0.4553630	4686 \pm 33	3.887 \pm 0.024	0.270 \pm 0.006	-50 \pm 1	5128 \pm 16	-0.155 \pm 0.018	9.37 \pm 0.05	0.35686 \pm 0.00431	0.9840	Q1
08215	0.5031375	8819 \pm 988	3.966 \pm 0.671	0.279 \pm 0.035	91 \pm 2	5408 \pm 38	0.429 \pm 0.155	5.07 \pm 0.36	0.10815 \pm 0.03036	0.5329	Q3
08442	0.5254550	3437 \pm 21	2.381 \pm 0.028	0.290 \pm 0.014	-138 \pm 2	5827 \pm 25	-0.211 \pm 0.027	7.87 \pm 0.10	0.15243 \pm 0.00499	0.6296	Q1
08697	0.5072340	2332 \pm 37	0.230 \pm 0.037	0.581 \pm 0.176	-106 \pm 10	7265 \pm 62	-0.298 \pm 0.006	1.82 \pm 2.45	0.00033 \pm 0.00021	0.0544	Q2
08752	0.6124250	3930 \pm 19	2.273 \pm 0.021	0.222 \pm 0.017	26 \pm 4	6088 \pm 43	0.375 \pm 0.021	6.45 \pm 0.07	0.10144 \pm 0.00295	0.5169	Q1
08830	0.5891080	4800 \pm 261	1.370 \pm 0.089	0.512 \pm 0.047	-8 \pm 4	5301 \pm 44	0.001 \pm 0.038	3.63 \pm 0.29	0.01501 \pm 0.00241	0.2258	Q3
09104	0.5150700	5438 \pm 47	1.501 \pm 0.014	0.489 \pm 0.011	-103 \pm 1	6028 \pm 16	0.026 \pm 0.007	3.44 \pm 0.03	0.01525 \pm 0.00030	0.2272	Q2
09276	0.5138700	5179 \pm 299	0.533 \pm 0.072	0.731 \pm 0.130	-98 \pm 14	6700 \pm 101	-0.195 \pm 0.030	2.31 \pm 3.13	0.00079 \pm 0.00038	0.0747	Q3
09577	0.5598490	2150 \pm 10	1.274 \pm 0.033	0.252 \pm 0.058	-114 \pm 11	6237 \pm 62	-0.926 \pm 0.020	6.67 \pm 0.22	0.05975 \pm 0.00470	0.4052	Q1
09635	0.5199447	3984 \pm 210	0.792 \pm 0.150	0.776 \pm 0.072	-175 \pm 5	7246 \pm 48	0.219 \pm 0.042	3.72 \pm 1.72	0.00468 \pm 0.00394	0.1433	Q3
09683	0.5992245	5383 \pm 392	1.722 \pm 0.133	0.278 \pm 0.058	-112 \pm 13	6774 \pm 156	0.077 \pm 0.057	3.63 \pm 0.09	0.02355 \pm 0.00243	0.2714	Q3
09698	0.4769498	5541 \pm 522	0.566 \pm 0.079	0.262 \pm 0.082	66 \pm 12	6487 \pm 150	0.125 \pm 0.044	1.15 \pm 0.08	0.00080 \pm 0.00022	0.0750	Q3
09778	0.4900290	3095 \pm 55	0.247 \pm 0.008	0.262 \pm 0.053	84 \pm 15	8767 \pm 144	0.089 \pm 0.007	0.90 \pm 0.03	0.00021 \pm 0.00002	0.0467	Q2
09781	0.6973228	3454 \pm 93	0.199 \pm 0.015	0.504 \pm 0.084	-170 \pm 10	6411 \pm 87	0.055 \pm 0.006	0.74 \pm 0.10	0.00009 \pm 0.00002	0.0348	Q2
09789	0.6461960	3718 \pm 7	2.774 \pm 0.021	0.222 \pm 0.011	93 \pm 2	8470 \pm 25	0.308 \pm 0.010	8.32 \pm 0.09	0.20605 \pm 0.00505	0.7333	Q1
10047	0.4859560	4520 \pm 323	0.405 \pm 0.060	0.110 \pm 0.074	3 \pm 32	4567 \pm 394	0.084 \pm 0.048	0.98 \pm 0.08	0.00044 \pm 0.00014	0.0607	Q3
10142	0.5082680	3734 \pm 18	2.120 \pm 0.014	0.105 \pm 0.007	129 \pm 4	5364 \pm 50	-0.713 \pm 0.013	6.21 \pm 0.03	0.09120 \pm 0.00141	0.4917	Q2
10158	0.6122545	4413 \pm 268	2.295 \pm 0.141	0.378 \pm 0.033	24 \pm 5	5634 \pm 51	-0.071 \pm 0.109	6.12 \pm 0.17	0.08294 \pm 0.00700	0.4705	Q3
10210	0.5681330	3500 \pm 51	0.725 \pm 0.023	0.487 \pm 0.034	-165 \pm 4	6838 \pm 32	-0.011 \pm 0.017	2.59 \pm 0.12	0.00416 \pm 0.00036	0.1371	Q2
10356	0.4942865	4965 \pm 366	2.614 \pm 0.246	0.441 \pm 0.027	114 \pm 4	6051 \pm 37	0.363 \pm 0.169	6.38 \pm 0.22	0.09677 \pm 0.01337	0.5056	Q3
10705	0.3599295	3427 \pm 28	0.864 \pm 0.019	0.134 \pm 0.034	-133 \pm 15	4241 \pm 149	-0.103 \pm 0.009	2.77 \pm 0.06	0.00733 \pm 0.00047	0.1702	Q1
10745	0.7294600	3768 \pm 29	1.073 \pm 0.019	0.160 \pm 0.030	62 \pm 9	8475 \pm 105	0.069 \pm 0.013	3.14 \pm 0.07	0.01160 \pm 0.00063	0.2037	Q1
10906	0.4920660	3719 \pm 60	0.280 \pm 0.009	0.308 \pm 0.049	-63 \pm 11	6409 \pm 112	0.040 \pm 0.003	0.86 \pm 0.03	0.00021 \pm 0.00002	0.0469	Q2
11090	0.5940300	7618 \pm 448	3.341 \pm 0.307	0.201 \pm 0.025	-118 \pm 4	5192 \pm 76	0.244 \pm 0.100	4.86 \pm 0.19	0.08609 \pm 0.01387	0.4786	Q3
11098	0.5121868	5823 \pm 506	0.470 \pm 0.055	0.575 \pm 0.071	25 \pm 8	5721 \pm 106	-0.012 \pm 0.030	1.08 \pm 0.10	0.00042 \pm 0.00011	0.0594	Q3
11105	0.5204120	4022 \pm 78	0.287 \pm 0.012	0.507 \pm 0.051	-47 \pm 9	7255 \pm 81	-0.131 \pm 0.004	0.91 \pm 0.06	0.00020 \pm 0.00003	0.0457	Q2
11108	0.5983080	2877 \pm 28	0.685 \pm 0.045	0.629 \pm 0.119	-107 \pm 6	8725 \pm 41	-0.001 \pm 0.012	3.72 \pm 2.40	0.00527 \pm 0.00125	0.1499	Q2
11442	0.5145645	4739 \pm 177	0.392 \pm 0.010	0.508 \pm 0.033	-17 \pm 4	7335 \pm 45	0.070 \pm 0.004	1.05 \pm 0.03	0.00036 \pm 0.00003	0.0564	Q3

Table 1 continued

Table 1 (continued)

ID	P	P_{orb}	$a_1 \sin i$	e	ω	T_0	β	K_1	$f(m)$	$M_{\text{S,min.}}$	Quality
	(days)	(days)	(au)		(deg)	(days)	(day Myr $^{-1}$)	(km s $^{-1}$)	(M_{\odot})	(M_{\odot})	
11522	0.4216520	5114 \pm 24	0.817 \pm 0.009	0.567 \pm 0.015	11 \pm 1	8418 \pm 15	0.381 \pm 0.004	2.11 \pm 0.05	0.00278 \pm 0.00010	0.1180	Q2
11683	0.6346595	4999 \pm 51	2.375 \pm 0.028	0.290 \pm 0.017	-24 \pm 3	7045 \pm 44	-0.007 \pm 0.013	5.40 \pm 0.07	0.07154 \pm 0.00241	0.4396	Q1
11730	0.7360930	5405 \pm 288	3.355 \pm 0.313	0.266 \pm 0.083	45 \pm 19	8433 \pm 369	0.403 \pm 0.230	7.03 \pm 0.36	0.17387 \pm 0.03463	0.6724	Q3
11833	0.5625820	3238 \pm 11	1.865 \pm 0.009	0.272 \pm 0.010	-54 \pm 1	5911 \pm 15	0.039 \pm 0.011	6.51 \pm 0.05	0.08251 \pm 0.00121	0.4693	Q1
11966	0.5075527	6393 \pm 337	0.394 \pm 0.031	0.680 \pm 0.047	-59 \pm 7	6976 \pm 65	0.036 \pm 0.014	0.92 \pm 0.09	0.00020 \pm 0.00003	0.0460	Q3
11989	0.5023055	4073 \pm 62	0.397 \pm 0.017	0.312 \pm 0.080	30 \pm 13	7996 \pm 149	0.234 \pm 0.007	1.12 \pm 0.07	0.00050 \pm 0.00007	0.0636	Q2
11990	0.4938388	1896 \pm 28	0.139 \pm 0.007	0.199 \pm 0.101	81 \pm 39	6562 \pm 203	0.107 \pm 0.005	0.82 \pm 0.05	0.00010 \pm 0.00002	0.0361	Q2
12333	0.6085633	3206 \pm 39	0.748 \pm 0.019	0.061 \pm 0.038	-87 \pm 46	6378 \pm 411	0.043 \pm 0.011	2.55 \pm 0.07	0.00545 \pm 0.00044	0.1519	Q2
12343	0.5415900	3275 \pm 106	0.810 \pm 0.074	0.445 \pm 0.110	69 \pm 17	4893 \pm 185	0.247 \pm 0.042	3.05 \pm 0.44	0.00672 \pm 0.00165	0.1646	Q3
12466	0.4956910	4145 \pm 102	0.359 \pm 0.021	0.234 \pm 0.102	100 \pm 25	4562 \pm 298	-0.099 \pm 0.008	0.98 \pm 0.10	0.00036 \pm 0.00008	0.0567	Q3
12664	0.5169445	4476 \pm 96	0.834 \pm 0.042	0.516 \pm 0.049	-179 \pm 6	6505 \pm 57	-0.113 \pm 0.030	2.37 \pm 0.16	0.00388 \pm 0.00051	0.1335	Q2
12786	0.4816050	4884 \pm 80	0.556 \pm 0.017	0.315 \pm 0.045	17 \pm 7	8073 \pm 95	-0.008 \pm 0.012	1.31 \pm 0.04	0.00096 \pm 0.00008	0.0800	Q2
12819	0.5102775	3698 \pm 89	0.267 \pm 0.017	0.259 \pm 0.071	-146 \pm 25	7724 \pm 246	-0.099 \pm 0.007	0.82 \pm 0.06	0.00019 \pm 0.00004	0.0449	Q2
13159	0.5451018	3381 \pm 54	0.692 \pm 0.013	0.215 \pm 0.039	149 \pm 12	4710 \pm 140	0.089 \pm 0.009	2.28 \pm 0.05	0.00387 \pm 0.00023	0.1334	Q2
13260	0.5689770	3231 \pm 11	0.775 \pm 0.013	0.537 \pm 0.026	92 \pm 3	7656 \pm 23	0.121 \pm 0.006	3.10 \pm 0.09	0.00595 \pm 0.00029	0.1571	Q1
13454	0.7109620	1076 \pm 6	0.764 \pm 0.038	0.433 \pm 0.100	132 \pm 12	7969 \pm 44	0.053 \pm 0.022	8.67 \pm 0.85	0.05173 \pm 0.00841	0.3800	Q1
13477	0.5749995	4502 \pm 81	3.722 \pm 0.090	0.139 \pm 0.028	-30 \pm 8	5704 \pm 100	-0.010 \pm 0.075	9.08 \pm 0.14	0.33949 \pm 0.01569	0.9572	Q2
13534	0.4631050	3672 \pm 12	0.943 \pm 0.011	0.271 \pm 0.022	22 \pm 4	7455 \pm 41	0.003 \pm 0.004	2.90 \pm 0.04	0.00830 \pm 0.00030	0.1786	Q1
13896	0.6061850	3054 \pm 80	1.990 \pm 0.088	0.295 \pm 0.054	148 \pm 6	8687 \pm 66	-0.051 \pm 0.024	7.43 \pm 0.25	0.11289 \pm 0.01087	0.5439	Q2
14101	0.5837305	4097 \pm 38	1.126 \pm 0.041	0.423 \pm 0.050	-21 \pm 7	7891 \pm 59	-0.087 \pm 0.025	3.31 \pm 0.21	0.01139 \pm 0.00135	0.2022	Q2
14145	0.4727650	4066 \pm 12	2.303 \pm 0.041	0.443 \pm 0.021	-17 \pm 2	7148 \pm 30	0.252 \pm 0.006	6.88 \pm 0.19	0.09868 \pm 0.00522	0.5102	Q1
14526	0.6694710	2926 \pm 24	1.393 \pm 0.058	0.389 \pm 0.064	41 \pm 8	6185 \pm 66	0.152 \pm 0.028	5.65 \pm 0.39	0.04236 \pm 0.00549	0.3482	Q1
14784	0.5776860	2999 \pm 227	0.849 \pm 0.102	0.260 \pm 0.128	-169 \pm 37	7038 \pm 302	0.046 \pm 0.027	3.23 \pm 0.39	0.00928 \pm 0.00264	0.1866	Q3
14786	0.6100320	2332 \pm 56	1.290 \pm 0.076	0.352 \pm 0.070	-106 \pm 13	5237 \pm 91	-0.396 \pm 0.102	6.46 \pm 0.50	0.05299 \pm 0.00832	0.3841	Q3
14815	0.5610100	2798 \pm 85	0.297 \pm 0.035	0.477 \pm 0.127	156 \pm 15	6272 \pm 117	-0.173 \pm 0.014	1.36 \pm 0.32	0.00047 \pm 0.00020	0.0618	Q3
14830	0.6147847	4489 \pm 186	0.989 \pm 0.107	0.525 \pm 0.141	157 \pm 13	7007 \pm 145	-0.043 \pm 0.031	2.94 \pm 0.68	0.00666 \pm 0.00248	0.1640	Q2
14891	0.6368730	7525 \pm 524	2.730 \pm 0.430	0.169 \pm 0.060	131 \pm 17	8093 \pm 309	0.259 \pm 0.299	3.99 \pm 0.43	0.04939 \pm 0.01817	0.3723	Q3
14905	0.5214227	3627 \pm 76	0.324 \pm 0.033	0.447 \pm 0.145	-159 \pm 13	7513 \pm 131	-0.006 \pm 0.009	1.13 \pm 0.25	0.00036 \pm 0.00013	0.0562	Q2
15388	0.5010780	2919 \pm 29	2.095 \pm 0.085	0.407 \pm 0.088	-134 \pm 7	8269 \pm 63	0.361 \pm 0.028	8.63 \pm 0.75	0.14483 \pm 0.01943	0.6139	Q3
15394	0.4839540	3532 \pm 63	0.420 \pm 0.018	0.093 \pm 0.070	-65 \pm 90	7498 \pm 648	-0.171 \pm 0.010	1.30 \pm 0.07	0.00080 \pm 0.00011	0.0748	Q3
15784	0.6415150	3657 \pm 161	2.246 \pm 0.144	0.286 \pm 0.060	-93 \pm 17	7813 \pm 149	0.083 \pm 0.114	6.98 \pm 0.25	0.11356 \pm 0.01564	0.5455	Q3
15841	0.6605260	3411 \pm 83	2.104 \pm 0.107	0.141 \pm 0.062	-1 \pm 35	4044 \pm 359	0.528 \pm 0.045	6.79 \pm 0.31	0.10735 \pm 0.01427	0.5310	Q2
20376	0.7347950	1641 \pm 19	2.330 \pm 0.313	0.628 \pm 0.094	162 \pm 5	7657 \pm 25	3.687 \pm 0.179	20.75 \pm 6.38	0.66507 \pm 0.37041	1.4159	Q3
20627	0.4444910	1186 \pm 9	0.261 \pm 0.009	0.271 \pm 0.074	95 \pm 16	7507 \pm 54	0.114 \pm 0.014	2.49 \pm 0.12	0.00169 \pm 0.00018	0.0981	Q1
31312	0.4632650	2106 \pm 57	0.675 \pm 0.025	0.265 \pm 0.070	-29 \pm 13	7528 \pm 76	-0.074 \pm 0.084	3.63 \pm 0.18	0.00930 \pm 0.00092	0.1867	Q2

NOTE—The first two columns contain the OGLE ID (in the format OGLE-BLG-RRLYR- ID) and the period used to construct the $O - C$ diagrams of the variables. The second set of six columns provides estimates for the orbital period, projected semimajor axis, eccentricity, argument of periastron, time of periastron passage (in the format HJD-2,450,000) and period-change rate, respectively. Note that these six parameters and their associated uncertainties are derived directly from their marginalized posterior distributions given by the employed MCMC method. The following set of three columns give estimates for the expected radial velocity semiamplitude, the mass function, and the minimum mass of the companion. The first two of these quantities are calculated for each of the posterior samples given by the MCMC analysis, and their means and standard deviations are listed here. The minimum masses of the companion objects are shown for the mean estimates of the mass functions of the variables only, and were calculated assuming $m_{\text{RR}} \equiv 0.65 M_{\odot}$ and $i \equiv 90^\circ$. Finally, the last column indicates the quality class assigned to each of the variables, with Q1 being the most certain candidates for binary systems.

After the removal of the last few dubious cases, 87 stars remained on our final list. For these stars, the final posterior samples were determined by running EMCEE for 31,000 cycles with 200 walkers, utilizing the priors listed in the Appendix. After an initial burn-in of 1000 iterations, the remaining chains samples were thinned by a factor of 300, resulting in 20,000 samples of the posterior probability distributions for each of the variables.

Table 1 presents the result of our analysis: for each of the 87 variables, it gives the OGLE identifier and the period used to construct the $O - C$ diagram, along with estimates of var-

ious orbital parameters and derived quantities and their uncertainties. The first two of these, P_{orb} and $a_1 \sin i$, are derived directly as the means and standard deviations of their marginalized posterior distributions. The next two parameters, e and ω , are computed similarly, but only after transforming the $\sqrt{e} \sin \omega$ and $\sqrt{e} \cos \omega$ values of the chain using Equations 6 and 7. As ω is a circular quantity, special care is taken to keep the posterior estimates contiguous for the calculation of its mean and standard deviation, with the former quantity finally given in the range $[-180^\circ; 180^\circ]$. The final two quantities directly derived from the LTTE + parabola

fit, T_0 and the period-change rate β (after converting the c_2 values using Equation 5), are likewise given.

We also list some additional quantities derived from the orbital solutions. The semiamplitude of the expected radial velocity variation of the RRL due to the binarity, K_1 , can be expressed as

$$K_1 = \frac{2\pi a_1 \sin i}{P_{\text{orb}} \sqrt{1 - e^2}}, \quad (8)$$

which we have calculated for every posterior sample, with their averages and standard deviations being listed in Table 1. As we have no additional information on the inclinations or mass ratios of the systems, the only physical quantity we can still calculate is the mass function:

$$f(m) = \frac{a_1^3 \sin^3 i}{P_{\text{orb}} \sqrt{1 - e^2}}, \quad (9)$$

which itself is connected to the masses of the components through

$$f(m) = \frac{m_S^3 \sin^3 i}{(m_{\text{RR}} + m_S)^2}, \quad (10)$$

where m_{RR} and m_S are the masses of the RRL and the companion, respectively. Similarly to the estimation of the expected radial velocity, we calculate the mean and standard deviation of the mass function after calculating it for all samples of the posterior distributions, and these are listed in Table 1. Finally, we also list the minimum masses of the RRL companions, calculated through Equation 10 assuming $i \equiv 90^\circ$ and $m_{\text{RR}} \equiv 0.65M_\odot$, the latter being representative of typical values estimated with various methods (see, e.g., Sandage 1993; Bono et al. 1996 and Contreras Peña et al. 2018, as well as references therein).

As the quality of the MCMC solutions varies by a great deal between different RRL variables, we have less confidence in some of our candidates and therefore decided to indicate our degree of belief with an additional quality category, given in the last column of Table 1. A quality category of Q1 marks the best candidates, and all of them have orbital periods with uncertainties less than 1%. Candidates in category Q2 either have larger former relative errors than those of Q1, or there are discrepancies in their $O - C$ diagrams that cause us to be more cautious with their classification. The variables assigned a category of Q3 generally have problematic fits, in most cases due to the distribution or insufficient extent of the data, which prevents the accurate determination of their binary parameters. For example, in the case of 20376, it has a pulsational period-change rate four times larger than any other star in the sample, causing us to be cautious with

Table 2. RR Lyrae Previously Classified as Binary Candidates

ID	References	Quality	ID	References	Quality
01573	P19	NB	09023	P19	NB
02854	P19	Q1	09729	P19	NB
03357	P19	NB	09778	P19	Q2
04376	H15; P19	Q2	09789	H15	Q1
04522	H15 Table 1	NB	10891	H15 Table 1	NB
04628	P19	Q2	11522	H15	Q2
05089	P19	Q2	11683	H15 Table 1	Q1
05135	H15 Table 1	Q2	12333	P19	Q2
05152	H15 Table 1	Q2	12611	H15 Table 1	NB
05691	H15; P19	NB	12698	H15 Table 1	NB
06498	H15	Q1	13454	H18	Q1
06567	P19	NB	13477	P19	Q2
06981	H15; P19	Q1	13534	H15	Q1
07051	P19	Q2	14145	H15	Q1
07566	H15	Q1	14408	H15	NB
07640	H15; P19	Q1	14526	P19	Q1
07943	H15	Q1	14852	H15 Table 1	NB
08185	P19	Q1	14891	P19	Q3
08215	H18	Q3	20627	P19	Q1

NOTE—For each of the variables, the first two columns give the OGLE ID and the references to the work(s) where the star has been discussed previously. The references are: H15 – Hajdu et al. (2015); H15 Table 1 – Hajdu et al. (2015), but no binary solution presented, and the star is only listed in Table 1 of that work; H18 – Hajdu et al. (2018); P19 – Prudil et al. (2019). The last column gives the same quality information as Table 1, except that stars that are no longer considered to be likely binary candidates are marked as “NB.”

it. Nevertheless, we have decided to retain it, because the $O - C$ diagram extended with the last two years of OGLE-IV observations follows exactly the trend extrapolated from the fit using data from the preceding years only.

Figure 1 presents the $O - C$ diagrams of the 87 RRL binary candidates and their MCMC solutions, with dashed lines denoting the binary solutions according to the average marginalized posterior estimates of the parameters given in Table 1. Furthermore, the shaded areas give the ranges (credible intervals) containing $\sim 68.3\%$, $\sim 95.4\%$, and $\sim 99.7\%$ of $O - C$ solutions at any given point in time. The colors of these shaded areas denote the quality class assigned to a variable (green, yellow, and red for Q1, Q2, and Q3 in Table 1, respectively).

3.1. Previously announced candidates

Previous studies have uncovered a total of 38 binary candidates toward the Galactic bulge through the LTTE using $O - C$ diagrams. In the original study of Hajdu et al. (2015) we have presented 20 potential candidates, and provided binary parameters for 12 of them (eight more tentative candidates were listed in Table 1 of that study, with no binary parameters determined for them). Two more stars were pre-

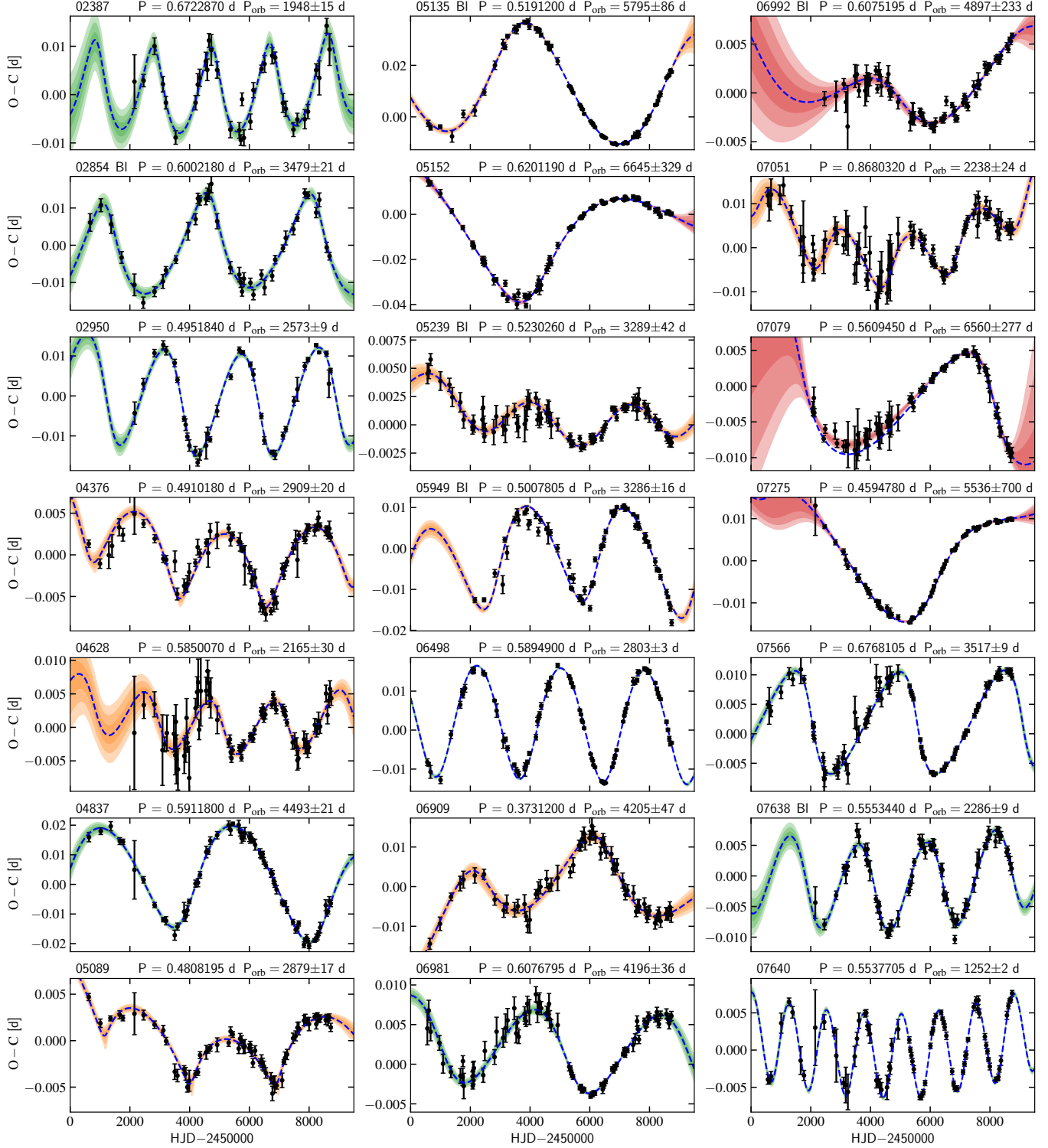


Figure 1. Final $O - C$ diagrams and their MCMC solutions. The shaded areas denote the ranges enclosing the fraction of posterior solutions corresponding to one, two, and three standard deviations (in order of decreasing transparency), while their color indicates which quality class has been assigned to the variable (green, yellow, and red for Q1, Q2, and Q3, respectively). The dashed blue line denotes the solution according to the mean parameters adopted from Table 1. The information given above each of the panels is the OGLE identifier of the RRL, the presence of the Blazhko effect in the light curve denoted by "BI", the period used for constructing the $O - C$ diagram, and the orbital period inferred from its MCMC solution.

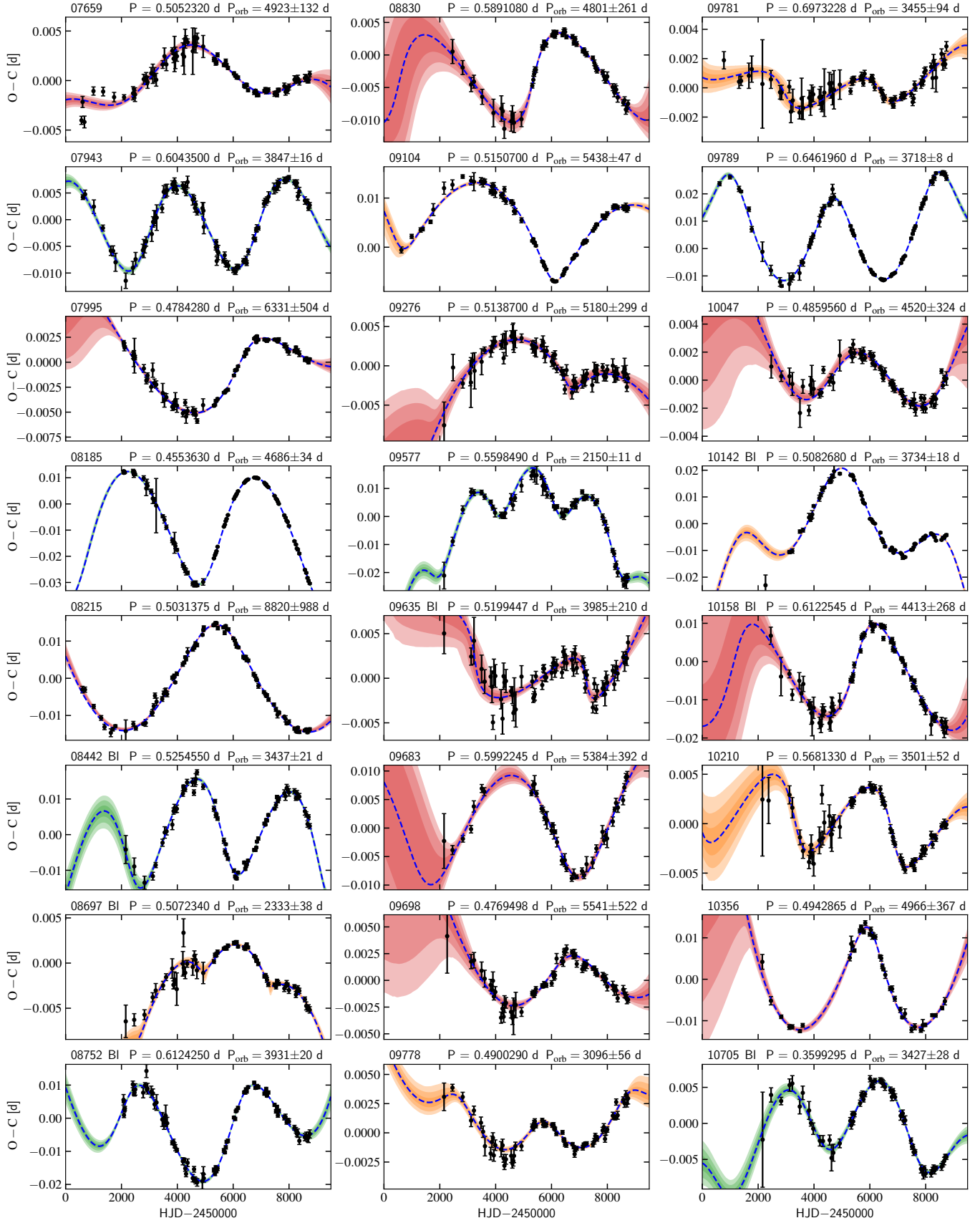


Figure 1. Continued from previous page.

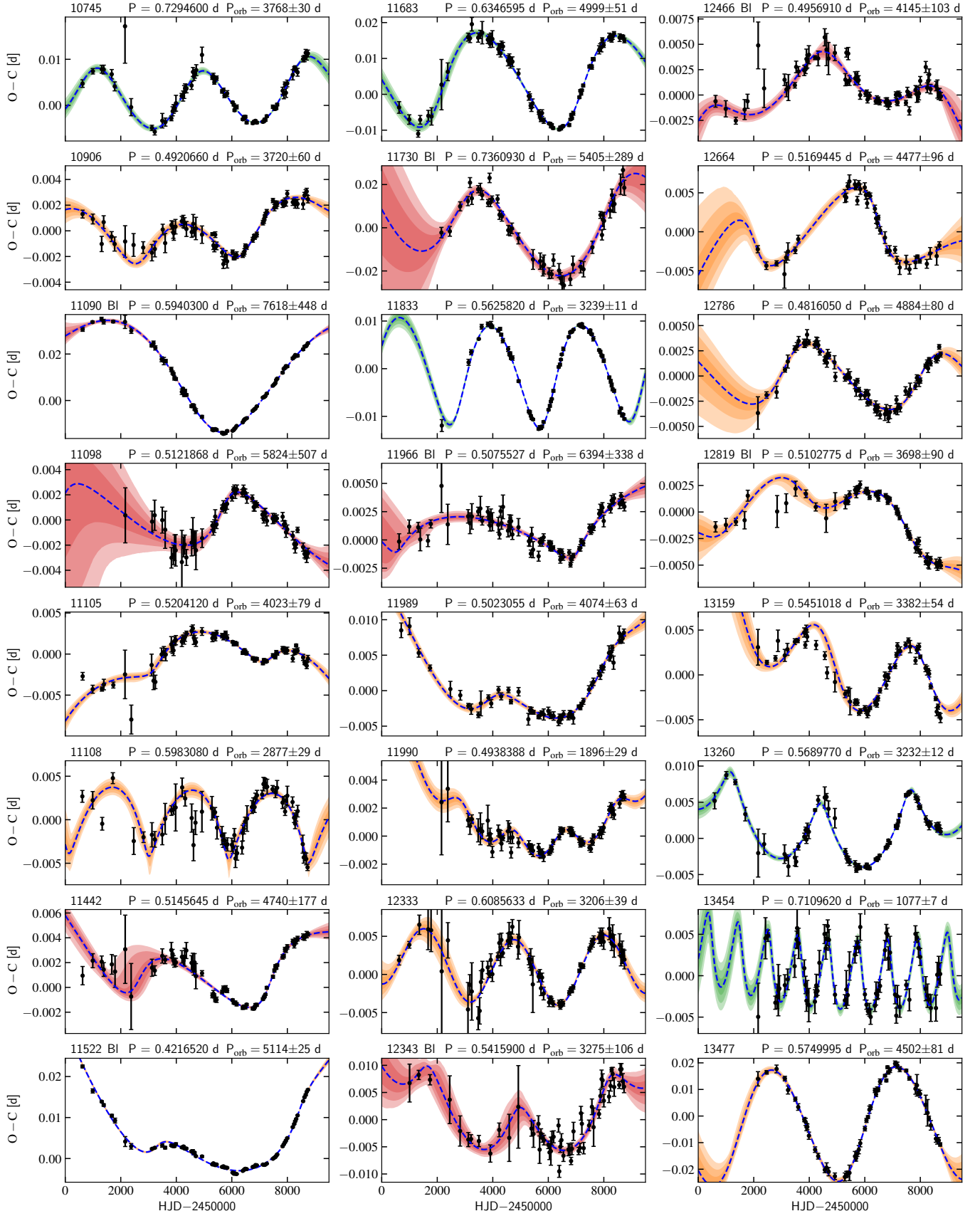


Figure 1. Continued from previous page.

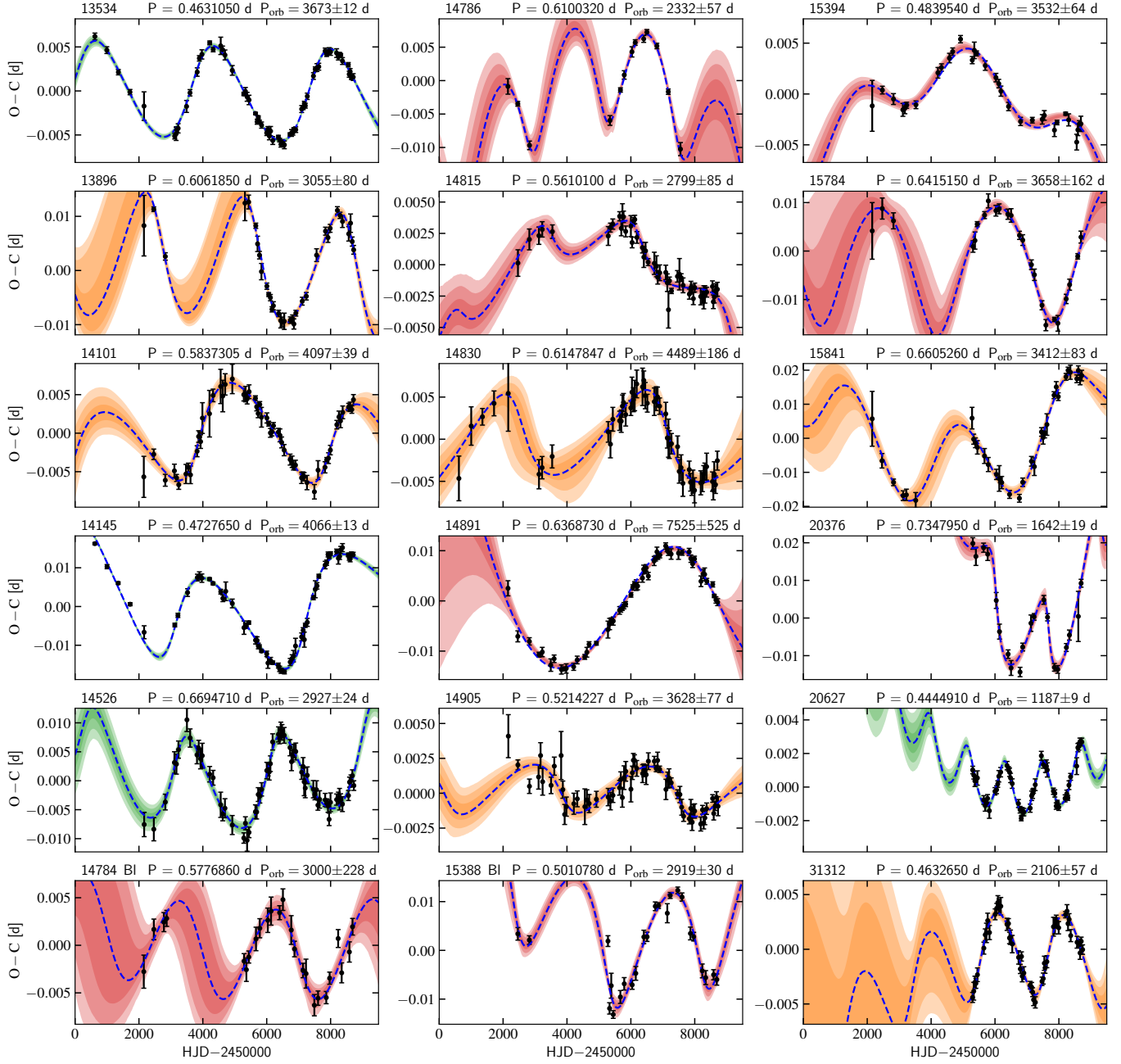


Figure 1. Continued from previous page.

sented as potential candidates in Fig. 2 of Hajdu et al. (2018). Finally, Prudil et al. (2019) reported the discovery of 20 additional candidates; however, four stars (04376, 05691, 06981, and 07640) had already been analyzed in Hajdu et al. (2015), leaving them with 16 new prospective binaries. All these variables were revised during our search, and the summarized findings are presented in Table 2.

During our analysis, we have discarded 12 former candidates from our list of binary RRL candidates for different reasons. Most commonly, the $O - C$ points of stars deviate from the prediction based on the previously available shorter data (01573, 06567, 09729), or the earlier and later parts of the $O - C$ diagram cannot be fit with an LTTE solution consistently (10891, 12611, 12698, 14408, 14852). We attribute these cases mostly to random period changes sometimes affecting RRL variables. In other instances, the analysis of the light curve revealed that the apparent cyclic $O - C$ behavior is caused by the Blazhko effect (04522, 05691). Finally, we were unable to recover the periodic shape of the $O - C$ diagram presented by Prudil et al. (2019) for two variables (03357 and 09023), while employing our $O - C$ procedure described in Section 2.

3.2. Blazhko effect and binarity

Studies of the long-term (decades or longer) behavior of the Blazhko effect are few and far between, and generally concern either individual, bright stars (e.g., XZ Dra: Jurcsik et al. 2002; RR Gem: Sódor et al. 2007; RV UMa: Hurta 2007; RZ Lyr: Jurcsik et al. 2012b; RR Lyr: Le Borgne et al. 2014) or RRLs in globular clusters (Messier 5: Jurcsik et al. 2011; Messier 3: Jurcsik et al. 2012a). The general image that has emerged through these studies is that changes (including the appearance or disappearance) of the Blazhko modulation are usually accompanied by changes in the pulsational period of the RRL (as traced with $O - C$ diagrams in most studies). If these changes are (quasi)periodic, they can mimic the signal expected from binarity, as shown by Skarka et al. (2018) in the case of Z CVn. It should be mentioned, however, that there are Blazhko stars without sudden period changes on a time scale of ~ 100 yr (e.g. DM Cyg, see Fig. 15 of Jurcsik et al. 2009a).

Besides affecting the pulsational period of RRL stars, the phase modulation of the light curve caused by the Blazhko effect can also be misinterpreted as a signal of binarity. As the modulation periods reach well into the range of expected orbital periods for RRL binaries,⁴ this is especially problematic in the case of studies making use of only timings of maxima. This is the exact reason why, as mentioned in Section 2.1, we have inspected the period change plus LTTE-corrected light

Table 3. Blazhko Periods Detected in the RR Lyrae Binary Candidates

ID	$P_{B1,1}$	$P_{B1,2}$	$P_{B1,Sk}$	Type
	(days)	(days)	(days)	
02854	18.50	67.01	—	—
05135	<i>12.63</i>	—	—	—
05239	10.68	—	—	—
05949	21.60	—	—	—
06992	354	—	—	—
07638	234.54	—	235.29	c
08442	19.31	167.45	19.33	a
08697	<i>31.72</i>	—	—	—
08752	27.30	51.50	27.29	a
09635	22.94	—	22.94	a
10142	23.52	—	238.10	—
10158	23.25	—	23.23	c
10705	7.01	—	7.01	a
11090	290.6	—	—	—
11522	16.14	—	—	—
11730	54.08	—	54.05	a
11966	26.33	—	—	—
12343	102.23	175.30	102.04	—
12466	23.16	17.28	23.15	a
12819	23.13	—	—	—
14784	20.62	—	—	—
15388	145.80	—	—	—

NOTE—For each of the variables, the meaning of the columns in order is: the OGLE ID; the first detected Blazhko period; the second detected Blazhko period; the Blazhko period reported by Skarka et al. (2020); and the latter authors' reported morphological type (both only if present in their Table 1). Blazhko periods with high uncertainty are marked in *italics*.

curves of each of the variables for signs of the Blazhko effect, and discarded those candidates whose detected Blazhko periods were similar to the suspected orbital period. This search (based mostly on the inspection of Fourier spectra of residual light curves for side peaks of the main harmonics of the pulsational frequency, as well as folded light curves and animations of the suspected modulation periods) has also revealed that 22 of the 87 candidates indeed exhibit the Blazhko effect (besides their modulation from LTTE). The modulation periods found are listed in Table 3, alongside their values and modulation classes (when present) previously published by Skarka et al. (2020). Generally, we find the same dominant modulation period, except for 10142, which admittedly has a somewhat complicated residual power spectrum, with multiple plausible periods. For five stars, we have also found a significant secondary modulation signal.

The frequency of RRLs showing the Blazhko effect is estimated to be $\sim 50\%$ (Jurcsik et al. 2009b; Kolenberg et al. 2010; Plachy et al. 2019), although recently there have been suggestions that all RRLs are in fact modulated, but a sig-

⁴ V144 in Messier 3 has a Blazhko period longer than 25 yr (Jurcsik & Smola 2016).

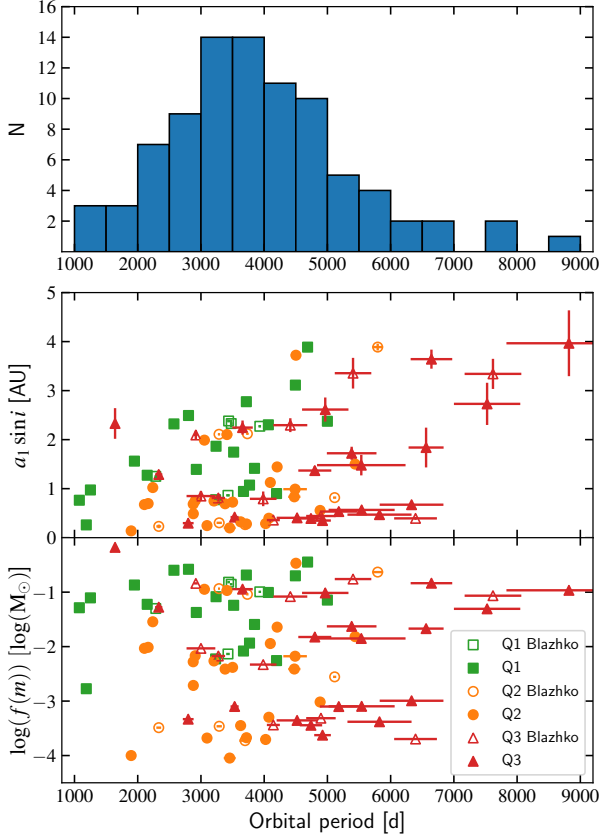


Figure 2. Top: orbital period distribution of the bulge RRL binary candidate sample. Middle: the distribution of the projected semimajor axes as a function of the orbital periods. Green squares, yellow circles, and red triangles denote variables with assigned quality of first, second, and third class, respectively, as listed in Table 1. Empty symbols indicate variables with presence of the Blazhko effect (Table 3). Bottom: same as the middle panel, but for the distribution of the (logarithmic) mass function from Table 1.

nificant fraction are modulated with very small amplitudes (Kovács 2018). The presence of the Blazhko effect can hinder the detection of the LTTE through its well-documented connection to sudden period changes, or by having a long-term phase modulation component, preventing the decoupling of the two effects. There are 65 stars where we do not detect its presence. Hence, if we adopt 50% as its incidence rate in RRL variables, we should have detected ~ 130 stars with LTTE. This also means that for variables afflicted by the presence of the Blazhko effect, the LTTE signal can still be recovered in $\sim 33\%$ of the cases. As the Blazhko effect prevents the detection of the LTTE signal in the remaining $\sim 66\%$ of affected variables, we can surmise that the binary nature of Blazhko variables can only be recovered in one third of cases.

4. STATISTICAL PROPERTIES OF THE CANDIDATE RR LYRAE BINARY POPULATION

For the first time, the sizable list of candidates presented in this work allows us to probe the population of RRLs in binaries, as well as to draw conclusions on their companion objects. The top panel of Figure 2 illustrates the distribution of orbital periods for the complete sample. The minimum period of ~ 1000 days is a hard limit on these objects, because not a single one has been detected by our search below this limit. It should be noted that with the method described in Section 2, we should have detected companions with orbital periods below 1000 days, if they existed. The frequency of binaries steadily increases from this limit up to periods of $\sim 3000 - 4000$ days, then decreases toward even longer periods. As the OGLE project evolved, the list of observed fields has been changed, sometimes resulting in shorter RRL light curves than the total possible baseline, mostly in OGLE-III.⁵ Gaps in the light curves prevent the discovery of longer-period binary RRLs in many cases, where it can be hard to decide whether the structure of the $O - C$ diagram is caused by the LTTE or by changes in the pulsation period. This is especially true for variables with low LTTE amplitudes, which, as described in Section 2.2, were discarded when it was not clear whether random period changes or the LTTE itself was causing the $O - C$ shapes. As can be seen in the middle panel of Figure 2, illustrating the distribution of semimajor axes, long-period, low-amplitude binaries are absent from the sample as a consequence. Furthermore, it can also be seen on this diagram that the maximum values of the projected semimajor axes seemingly increase with increasing periods. As illustrated by the distribution of mass-function values in the bottom panel of Figure 2, this roughly equates to an upper limit for the mass function, which in turn hints at a limit for the companion masses of RRL binaries.

The top panel of Figure 3 illustrates the distribution of eccentricities for the RRL binary candidate sample. Although the uncertainties on individual values are somewhat high for some of the candidates (as listed in Table 1), random fluctuations cannot explain the most prominent visible feature, the peak in the bin $0.25 < e < 0.3$. This bin contains ~ 4 times as many candidates as the average for other bins between 0.05 and 0.6. Supposing a Poisson distribution with a mean measured in these bins, the probability of a single bin (i.e., that of $0.25 < e < 0.3$) having more than 20 systems is less than 10^{-6} . Furthermore, systems with eccentricities higher than 0.6 appear to be exceedingly rare (only six candidates, or 7% of the total sample).

The distribution of the derived mass-function values for the sample of RRL binary candidates is shown in the middle panel of Figure 3 (on a logarithmic scale). The distribu-

⁵ This can be clearly seen in the $O - C$ diagrams in Figure 1 for, e.g., 13896, 14784, 14786, and 14815, among others.

tion is strikingly trimodal, strongly suggesting the presence of three dominant underlying populations of companions to RRL variables in binary systems. While we cannot derive the masses of individual companions from the information provided by LTTE alone, we can calculate the expected distribution of their $f(m)$ values through Equation 10, by assuming the same mass for all RRL components (adopted here as $0.65 M_{\odot}$, see Section 3), and an isotropic inclination distribution. We have found that under these conditions, dominant companion masses of ~ 0.6 , ~ 0.2 , and $\sim 0.067 M_{\odot}$ are able to reproduce the location, and to a lesser extent the shape, of these three peaks. It should be noted that if the adopted mean RRL mass is decreased to $0.55 M_{\odot}$, or increased to $0.75 M_{\odot}$, the dominant companion masses likewise decrease or increase by about $\sim 10\%$ for all three groups.

The bottom panel of Figure 3 illustrates the relation between the derived eccentricities and mass functions for the RRL binary candidates. While the low number of candidates complicates interpretation, it can still be surmised that all three mass-function groups contribute to the excess of variables with $0.25 < e < 0.3$. The group with the highest $f(m)$ values seems to have a roughly uniform underlying distribution between eccentricities of ~ 0.1 and ~ 0.5 . In contrast, the groups with lower $f(m)$ values show a paucity of eccentricity values around ~ 0.4 and a less significant excess around ~ 0.5 .

5. DISCUSSION

As already demonstrated in this study, the analysis of the $O-C$ diagram, when coupled with the modified [Hertzsprung \(1919\)](#) method presented in Section 2, is a powerful tool for the discovery of RRL binary candidates. Inspecting the presented $O-C$ diagrams, we can notice some general trends. For example, in the case of some variables (04376, 06498, and 09577) with more than two completed orbits, at some time intervals the $O-C$ points are systematically above the $O-C$ solutions while at others they are below. This phenomenon is most probably caused by the nonlinear change in the pulsational periods of the variables themselves. With continued observations, it will be possible to model this by extending the polynomial part of Equation 4 to higher orders, as was done by [Groenewegen & Jurkovic \(2017\)](#) in the case of Type II and anomalous Cepheids.

As we have adopted the Bayesian formalism with MCMC analysis, we can evaluate possible correlations between the binarity parameters using the distribution of posterior probabilities. Most candidates with long binary periods compared to the length of the available data (i.e., 07079, 07995, 08830, 09683, etc.) show diverging solutions (the shaded areas) in their $O-C$ diagrams. This is the result of a degeneracy between the pulsational period-change rates, the orbital periods,

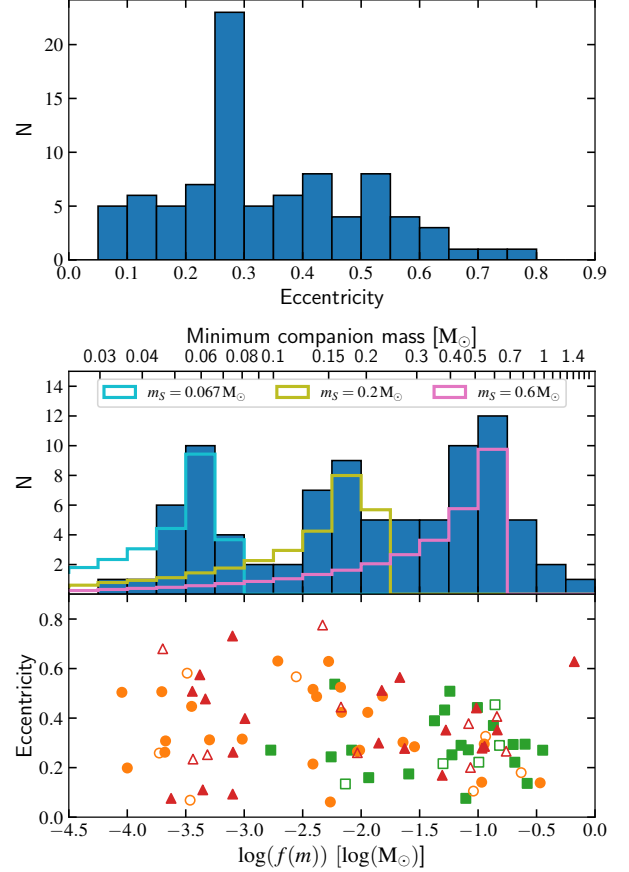


Figure 3. Top: eccentricity distribution of the bulge RRL binary candidate sample. Middle: distribution of the (logarithmic) mass function. In addition, the purple, yellow, and cyan lines show the expected mass-function distribution for companion masses of 0.6 , 0.2 , and $0.067 M_{\odot}$, respectively, selected to reproduce the three modes of the observed sample. Note that the top axis shows the minimum companion mass calculated for an assumed RRL mass of $0.65 M_{\odot}$. Bottom: the dependence of eccentricities on the (logarithmic) mass function in the bulge RRL binary sample. The meaning of the symbols is the same as in Figure 2.

and the projected semimajor axis, because a variety of combinations of these three parameters can reproduce the same shape for short segments of the $O-C$ curves (Equation 4). Although this prevents the derivation of accurate binary parameters, reflected in the classification of these stars as quality category Q3, as well as in the large relative errors given for these parameters in Table 1, the characteristic shape of the LTTE on the $O-C$ diagrams still allows their identification as binary candidates.

Another advantage of the adopted Bayesian formalism (albeit not yet used in this work) is that it can naturally include external information through the appropriate selection of priors. For example, if any of our candidates were to show even a single eclipse, the time of the eclipse could be converted to a prior through the times of inferior ($\omega + \nu = 90^\circ$) or superior

($\omega + \nu = 270^\circ$) conjunctions, providing a strong constraint on the binary parameters. The best known example for such a system is the binary Cepheid OGLE-SMC-CEP-3235 (see Fig. 2 in Udalski et al. 2015b), showing both a clear LTTE in its $O - C$ diagram and a single eclipse.

5.1. The nature of RRL companions

As RRL stars are Population II objects, the properties of their companions can provide important information about star formation in conditions no longer observable in the Milky Way. The distribution of mass-function values presented in Figure 3 provides strong clues toward this goal. There are three RRL binary candidates with estimated minimum companion masses higher than $0.95 M_\odot$, that is, similar to or higher than the expected masses of main-sequence progenitors of RRL variables. These systems are the current best candidates for RRL binaries containing high-mass degenerate companions. Stancliffe et al. (2013) modeled wind-driven accretion of material enhanced in carbon and neutron-capture elements onto stars that eventually form RRL variables from their higher-mass, more evolved AGB companions. This scenario could be verified if some of our RRL binary candidates were to show enhancement of these elements in their spectra. Whether there would be a chemical signature associated with neutron star or black hole companions should also be investigated. Alternatively, a more mundane scenario with hierarchical triple systems, containing two low-mass main-sequence companions in a tight binary, accompanied by the RRL star on a wider orbit, can also explain these high minimum companion masses.

As shown in Figure 3, the three modes of the mass-function distribution can be modeled with typical companion masses belonging to three distinct companion populations. In the globular cluster Messier 4 (NGC 6121), which itself contains a sizable population of RRL variables, the youngest single white dwarfs have masses of $\sim 0.53 M_\odot$ (Kalirai et al. 2009). This mass constitutes a lower limit on the masses of degenerate companions to RRL variables, under the assumption of no interaction between the components in the system. Older white dwarfs, the remnants of initially (at the formation of the system) higher-mass companions, are expected to follow the initial-final mass relation (IFMR; Cummings et al. 2018). The IFMR itself is quite flat, i.e., the final masses of white dwarfs around $\sim 0.6 M_\odot$ change little for a relatively wide range of initial masses (e.g., $\sim 0.57 M_\odot$ and $\sim 0.65 M_\odot$ for $1 M_\odot$ and $2 M_\odot$, respectively, according to Equation 4 in Cummings et al. 2018). The white dwarf mass distribution observed in the field supports this argument (Kepler et al. 2007). Hence, we surmise that the peak corresponding to the highest-mass companions in Figure 3 probably contains a significant population of white dwarf remnants of initially higher-mass ($1\text{--}2 M_\odot$) companions, with the rest

having companions still on the main sequence. However, the relative fraction of these two companion populations is not yet clear and will require further study.

White dwarfs with extremely low masses (ELMs; $\sim 0.2 M_\odot$) have been observed in the field (Liebert et al. 2004) and in binary systems (Masuda et al. 2019), and are generally thought to form through binary interaction. Therefore, it is tempting to attribute the middle-mass group ($\sim 0.2 M_\odot$) of RRL companions seen in Figure 3 to these objects. However, considering the long binary periods of these systems, the RRL progenitor probably did not interact with its companion. Instead, to facilitate the binary interaction scenario, a third object is required in the system in an initially close orbit with the supposed ELM progenitor. However, this third body would contribute its mass to that of the ELM to produce an LTTE bigger than observed in the light curve of the RRL variables, unless it was somehow ejected from the system. Alternatively, companions in this mass group might be ordinary M dwarfs, signaling a peculiar distribution distribution of mass ratio (q) in Population II binaries, with a strong peak at $q \sim 0.2$. This would mean that the mass ratio distribution for low-mass Population II binaries is very different from the mostly smooth and flat distribution observed for solar-type stars in the solar neighborhood for similar orbital periods (see fig. 30 of Moe & Di Stefano 2017).

The existence of the low-mass group (located at $\sim 0.067 M_\odot \approx 70 M_{\text{Jup}}$) is arguably the most puzzling feature of the mass-function distribution. These candidate companions are situated firmly in the brown dwarf (BD) mass regime ($\lesssim 0.075 M_\odot$; Burrows et al. 1997). Population II BDs are very faint objects, and as such, very few have been detected in the Galactic field (see, e.g., Zhang et al. 2017). Furthermore, very few extended radial velocity surveys of low-metallicity stars have been carried out, with the notable exception of the APOGEE observations (Troup et al. 2016; Price-Whelan et al. 2020). Nevertheless, most of the BD candidates detected in APOGEE have much shorter orbital periods than the ones presented here. Therefore, the detection of RRL binary candidates containing these objects may provide us with valuable information on the binarity of Population II BDs, which is not easily attainable through other methods.

Regardless of the nature of a companion, a binary system containing an RRL variable has necessarily undergone at least some evolution in its parameters as a consequence of mass loss on the red giant branch. Considerable effort toward binary evolution modeling and population synthesis studies are needed to recover the distributions of the original stellar and binary parameters of these objects. Nevertheless, they offer us a rather unique look into properties of the slightly subsolar mass stars of Population II.

On the observational side, continued photometric monitoring will result in extended $O-C$ diagrams and more accurate binary parameters. However, radial velocity observations are still necessary to verify at least a subset of the candidates of each $f(m)$ group, before they can be used to draw firm conclusions about the binary parameters of Population II. This will be especially challenging for the candidates with the lowest-mass companions, because the expected radial velocity semi-amplitudes listed in Table 1 are $\sim 1 \text{ km s}^{-1}$. These are overlaid on the large radial velocity variations caused by the pulsation of RRL stars (up to $\sim 60 \text{ km s}^{-1}$; see e.g., Fig. 3 of Jurcsik et al. 2017), hence the verification of these binary systems poses considerable challenge.

ACKNOWLEDGMENTS

The research leading to these results has received funding from the European Research Council (ERC) under the European Union’s Horizon 2020 research and innovation program (grant agreement No. 695099). We also acknowledge support from the National Science Center, Poland grants MAESTRO UMO-2017/26/A/ST9/00446, MAESTRO 2016/22/A/ST9/00009 and DIR/WK/2018/09 grants of the Polish Ministry of Science and Higher Education. The OGLE project has received funding from the National Science Centre, Poland, grant MAESTRO 2014/14/A/ST9/00121 to AU. J.J. acknowledges support from the OTKA grants NN-129075 and K-129249. Support for M.C. is provided by the Ministry for the Economy, Development, and Tourism’s Millennium Science Initiative through grant IC 12009, awarded to the Millennium Institute of Astrophysics (MAS) by Proyecto Basal AFB-170002; and by FONDECYT grant #1171273.

Facilities: OGLE.

Software: emcee (Foreman-Mackey et al. 2013), ChainConsumer (Hinton 2016), Jupyter (Kluyver et al. 2016), Numba (Lam et al. 2015), NumPy (Harris et al. 2020), SciPy (Virtanen et al. 2020), scikit-learn (Pedregosa et al. 2011)

APPENDIX

A. PRIORS UTILIZED DURING THE MCMC ANALYSIS

A critical step in the application of Bayesian statistics is the choice of prior distributions. For the three parameters of the parabolic component in Eq. 4, c_0 , c_1 , and c_2 , we apply uniform priors within the ranges of $[-1; 1]$, $[-10^{-4}; 10^{-4}]$, and $[-10^{-8}; 10^{-8}]$, respectively. The projected semi-major axis $a_1 \sin i$ is also constrained with a uniform prior to $[0; 10]$ (AU) for most stars, with the only exception being 20376, where this was modified to $[0; 5]$ (au) to avoid degenerate posterior samples with really large $a_1 \sin i$ values.

In order to determine appropriate ranges for the priors on the orbital period and the time of periastron passage, we make use of their values determined during the first iteration of the $O-C$ method: for the former, we adopt a default uniform prior in the range $[0.9 \times P_{\text{orb},1}; 1.1 \times P_{\text{orb},1}]$; for the latter, in $[T_{0,1} - 0.25 \times P_{\text{orb},1}; T_{0,1} + 0.25 \times P_{\text{orb},1}]$, where

$P_{\text{orb},1}$ and $T_{0,1}$ are the estimates for the quantities from the first iteration of the $O-C$ method. It should be noted that T_0 is a periodic (circular) quantity with a period of P_{orb} , hence the choice of these (default) constraints. We adopted flat priors of $[-1; 1]$ on the transformed quantities $\sqrt{e} \sin \omega$ and $\sqrt{e} \cos \omega$, resulting in an effective flat prior on e in the range of $[0; 1]$ (after converting them through Eq. 6).

There are two additional implicit “priors” utilized during the analysis, that is, they are necessary to reproduce the MCMC fits presented in Table 1 and Figure 1: the orders of the Fourier series used during the first and second iterations of the $O-C$ method employed here. Therefore, we list these parameters, along with the uniform prior ranges on P_{orb} and T_0 , in Table A1.

REFERENCES

- Beaton, R. L., Bono, G., Braga, V. F., et al. 2018, *SSRv*, 214, 113, doi: 10.1007/s11214-018-0542-1
- Blažko, S. 1907, *Astronomische Nachrichten*, 175, 325, doi: 10.1002/asna.19071752002

Table A1. Fourier orders and priors used to derive the final RRL binary parameters

ID	\mathcal{F}_1	\mathcal{F}_2	$P_{\text{orb,min.}}$	$P_{\text{orb,max.}}$	$T_{0,\text{min.}}$	$T_{0,\text{max.}}$	ID	\mathcal{F}_1	\mathcal{F}_2	$P_{\text{orb,min.}}$	$P_{\text{orb,max.}}$	$T_{0,\text{min.}}$	$T_{0,\text{max.}}$
02387	8	10	1766.6	2159.2	8295.3	9276.7	10705	10	15	3085.0	3564.9	3800.0	5000.0
02854	10	15	3133.3	3829.6	7345.0	9085.7	10745	15	20	3272.3	3999.4	7293.3	9111.2
02950	10	15	2295.5	2805.7	5764.0	7039.3	10906	10	15	3333.1	4073.7	5830.4	7682.1
04376	10	15	2610.6	3190.8	5798.9	7249.2	11090	10	15	5599.2	8398.8	3414.1	6913.6
04628	10	15	1887.0	2306.3	6723.1	7553.0	11098	10	15	4188.4	6515.3	4368.9	7083.6
04837	10	15	4058.6	4960.5	2700.1	4954.8	11105	10	15	3600.0	4400.0	6330.0	8330.0
05089	10	15	2593.9	3170.3	6267.6	7708.7	11108	10	15	2604.6	3183.4	8001.9	9448.9
05135	10	15	5201.7	6357.6	1992.2	4882.0	11442	10	15	4201.7	5602.2	6559.9	8894.2
05152	10	15	5941.6	7262.0	2478.7	5779.6	11522	10	15	4544.0	5553.8	7085.9	9610.3
05239	10	15	2949.7	3605.1	4044.1	6502.2	11683	10	15	4530.3	5537.0	5684.8	8201.6
05949	10	15	2935.1	3587.4	5223.3	6853.9	11730	8	10	4715.8	6287.7	7017.5	9637.4
06498	10	15	2518.7	3078.4	5812.7	7212.0	11833	10	20	2971.9	3632.3	5065.1	6716.2
06909	6	8	3798.2	4642.3	5445.9	7556.0	11966	10	15	4537.6	6806.5	5910.4	8746.4
06981	10	15	3834.4	4686.5	4204.9	6335.1	11989	10	15	3711.3	4536.0	7184.4	9246.3
06992	10	15	3952.6	5270.1	3434.1	5630.0	11990	10	15	1721.4	2104.0	5835.8	7270.3
07051	10	15	2035.9	2488.4	6224.9	7356.0	12333	10	15	2944.6	3599.0	5382.4	7563.6
07079	10	15	6042.1	7384.8	6435.9	9792.6	12343	10	15	2595.1	3892.6	3979.3	5601.2
07275	10	15	4800.0	9600.0	4119.1	8119.1	12466	10	15	3275.2	4912.7	3155.0	5543.2
07566	10	15	3167.7	3871.6	4704.4	6464.2	12664	10	15	4131.6	5049.8	5331.6	7627.0
07638	10	15	2050.7	2506.4	5955.4	7094.7	12786	10	15	4391.8	5367.8	6876.5	9316.4
07640	10	15	1133.7	1385.7	7960.1	8589.9	12819	10	15	2680.4	4467.3	6036.1	8642.0
07659	10	15	4302.9	5737.2	7058.8	9847.7	13159	10	15	3145.7	3844.8	3602.5	5350.1
07943	10	15	3437.0	4200.8	5534.8	7444.2	13260	10	15	2908.8	3555.2	6839.4	8455.5
07995	10	15	5007.2	7232.7	5026.8	7808.6	13454	10	15	961.4	1175.0	7641.2	8175.3
08185	10	15	4199.1	5132.2	3974.5	6307.3	13477	10	15	4251.4	5196.1	4491.5	6853.4
08215	10	15	5977.7	10461.0	3753.0	7489.1	13534	10	15	3277.2	4005.5	6515.3	8336.0
08442	10	15	3056.8	3736.0	5005.3	6703.5	13896	10	15	2675.8	3270.4	7895.0	9381.6
08697	10	15	2061.7	2519.8	6684.2	7829.5	14101	10	15	3691.4	4511.7	6782.7	8833.5
08752	10	15	3515.0	4296.1	5113.8	7066.6	14145	10	15	3677.7	4495.0	6302.5	8345.7
08830	10	15	4295.0	5249.5	4148.5	6534.6	14526	10	15	2621.2	3203.7	5453.9	6910.1
09104	10	15	4944.5	6043.3	4733.3	7480.2	14784	8	15	2353.2	3529.8	5981.7	8187.8
09276	10	15	4661.6	5697.5	5394.1	7983.8	14786	10	15	2078.6	2540.5	4644.0	5798.8
09577	10	15	1921.2	2348.2	5804.4	6871.7	14815	10	15	2441.2	3255.0	5550.9	6907.1
09635	10	15	3309.2	4780.0	6280.1	8118.6	14830	10	15	3918.7	5225.0	5831.3	8008.3
09683	10	15	4222.5	6099.2	5900.0	8245.9	14891	10	15	5695.9	8227.4	6526.9	9691.2
09698	10	15	3985.7	6293.2	5848.3	7200.0	14905	10	15	3373.1	4122.7	6855.6	8729.6
09778	10	15	2734.2	3341.7	7648.8	9420.9	15388	10	15	2626.9	3210.7	7568.6	9028.0
09781	15	20	2938.9	4041.0	5489.7	7326.5	15394	10	15	3159.6	3861.7	6514.7	8855.1
09789	10	15	3337.6	4079.3	7241.4	9713.7	15784	10	15	2896.6	4344.8	6714.5	8826.6
10047	10	15	3530.5	5099.7	3708.5	5669.9	15841	10	15	3003.5	3671.0	2900.0	5400.0
10142	10	15	3278.4	4507.8	4891.7	6940.7	20376	5	10	1483.6	1813.3	7241.2	8065.4
10158	10	15	3548.5	5322.7	4572.6	6790.4	20627	10	15	1069.1	1306.7	7195.4	7888.4
10210	10	15	3144.5	3843.3	6016.1	7763.0	31312	10	15	1860.2	2273.6	7019.7	8053.2
10356	10	15	3788.6	5682.9	4583.8	7740.9	—	—	—	—	—	—	—

Bono, G., Caputo, F., Castellani, V., & Marconi, M. 1996, ApJL, 471, L33, doi: [10.1086/310320](https://doi.org/10.1086/310320)

Burrows, A., Marley, M., Hubbard, W. B., et al. 1997, ApJ, 491, 856, doi: [10.1086/305002](https://doi.org/10.1086/305002)

Clementini, G., Ripepi, V., Molinaro, R., et al. 2019, A&A, 622, A60, doi: [10.1051/0004-6361/201833374](https://doi.org/10.1051/0004-6361/201833374)

Contreras Peña, C., Catelan, M., Grundahl, F., Stephens, A. W., & Smith, H. A. 2018, AJ, 155, 116, doi: [10.3847/1538-3881/aaa95e](https://doi.org/10.3847/1538-3881/aaa95e)

Cummings, J. D., Kalirai, J. S., Tremblay, P. E., Ramirez-Ruiz, E., & Choi, J. 2018, ApJ, 866, 21, doi: [10.3847/1538-4357/aadfd6](https://doi.org/10.3847/1538-4357/aadfd6)

Dékány, I., & Grebel, E. K. 2020, ApJ, 898, 46, doi: [10.3847/1538-4357/ab9d87](https://doi.org/10.3847/1538-4357/ab9d87)

Derekas, A., Kiss, L. L., Udalski, A., Bedding, T. R., & Szatmáry, K. 2004, MNRAS, 354, 821, doi: [10.1111/j.1365-2966.2004.08242.x](https://doi.org/10.1111/j.1365-2966.2004.08242.x)

Ferguson, P. S., & Strigari, L. E. 2020, MNRAS, 495, 4124, doi: [10.1093/mnras/staa1404](https://doi.org/10.1093/mnras/staa1404)

Foreman-Mackey, D., Hogg, D. W., Lang, D., & Goodman, J. 2013, PASP, 125, 306, doi: [10.1086/670067](https://doi.org/10.1086/670067)

- Goodman, J., & Weare, J. 2010, *Communications in Applied Mathematics and Computational Science*, 5, 65, doi: [10.2140/camcos.2010.5.65](https://doi.org/10.2140/camcos.2010.5.65)
- Groenewegen, M. A. T., & Jurkovic, M. I. 2017, *A&A*, 603, A70, doi: [10.1051/0004-6361/201730687](https://doi.org/10.1051/0004-6361/201730687)
- Guggenberger, E., Barnes, T. G., & Kolenberg, K. 2016, *Communications of the Konkoly Observatory Hungary*, 105, 145. <https://arxiv.org/abs/1512.00873>
- Guggenberger, E., & Steixner, J. 2015, in *European Physical Journal Web of Conferences*, Vol. 101, *European Physical Journal Web of Conferences*, 06030, doi: [10.1051/epjconf/201510106030](https://doi.org/10.1051/epjconf/201510106030)
- Hajdu, G., Catelan, M., Jurcsik, J., et al. 2015, *MNRAS*, 449, L113, doi: [10.1093/mnras/ltv024](https://doi.org/10.1093/mnras/ltv024)
- Hajdu, G., Catelan, M., Jurcsik, J., & Thompson, I. B. 2018, in *The RR Lyrae 2017 Conference. Revival of the Classical Pulsators: from Galactic Structure to Stellar Interior Diagnostics*, ed. R. Smolec, K. Kinemuchi, & R. I. Anderson, Vol. 6, 248–252
- Hansen, C. J., Nordström, B., Bonifacio, P., et al. 2011, *A&A*, 527, A65, doi: [10.1051/0004-6361/201015076](https://doi.org/10.1051/0004-6361/201015076)
- Harris, C. R., Millman, K. J., van der Walt, S. J., et al. 2020, *Nature*, 585, 357, doi: [10.1038/s41586-020-2649-2](https://doi.org/10.1038/s41586-020-2649-2)
- Hernitschek, N., Cohen, J. G., Rix, H.-W., et al. 2018, *ApJ*, 859, 31, doi: [10.3847/1538-4357/aabfbb](https://doi.org/10.3847/1538-4357/aabfbb)
- Hertzprung, E. 1919, *Astronomische Nachrichten*, 210, 17, doi: [10.1002/asna.19202100202](https://doi.org/10.1002/asna.19202100202)
- Hey, D. R., Murphy, S. J., Foreman-Mackey, D., et al. 2020, *AJ*, 159, 202, doi: [10.3847/1538-3881/ab7d38](https://doi.org/10.3847/1538-3881/ab7d38)
- Hinton, S. R. 2016, *The Journal of Open Source Software*, 1, 00045, doi: [10.21105/joss.00045](https://doi.org/10.21105/joss.00045)
- Hurta, Z. 2007, *Astronomische Nachrichten*, 328, 841, doi: [10.1002/asna.200710815](https://doi.org/10.1002/asna.200710815)
- Irwin, J. B. 1952, *ApJ*, 116, 211, doi: [10.1086/145604](https://doi.org/10.1086/145604)
- . 1959, *AJ*, 64, 149, doi: [10.1086/107913](https://doi.org/10.1086/107913)
- Jacyszyn-Dobrzeńicka, A. M., Skowron, D. M., Mróz, P., et al. 2017, *AcA*, 67, 1, doi: [10.32023/0001-5237/67.1.1](https://doi.org/10.32023/0001-5237/67.1.1)
- Jurcsik, J., Benko, J. M., & Szeidl, B. 2002, *A&A*, 396, 539, doi: [10.1051/0004-6361:20021301](https://doi.org/10.1051/0004-6361:20021301)
- Jurcsik, J., Clement, C., Geyer, E. H., & Domsa, I. 2001, *AJ*, 121, 951, doi: [10.1086/318746](https://doi.org/10.1086/318746)
- Jurcsik, J., & Smitola, P. 2016, *Communications of the Konkoly Observatory Hungary*, 105, 167
- Jurcsik, J., Szeidl, B., Clement, C., Hurta, Z., & Lovas, M. 2011, *MNRAS*, 411, 1763, doi: [10.1111/j.1365-2966.2010.17817.x](https://doi.org/10.1111/j.1365-2966.2010.17817.x)
- Jurcsik, J., Hurta, Z., Sódor, Á., et al. 2009a, *MNRAS*, 397, 350, doi: [10.1111/j.1365-2966.2009.14919.x](https://doi.org/10.1111/j.1365-2966.2009.14919.x)
- Jurcsik, J., Sódor, Á., Szeidl, B., et al. 2009b, *MNRAS*, 400, 1006, doi: [10.1111/j.1365-2966.2009.15515.x](https://doi.org/10.1111/j.1365-2966.2009.15515.x)
- Jurcsik, J., Hajdu, G., Szeidl, B., et al. 2012a, *MNRAS*, 419, 2173, doi: [10.1111/j.1365-2966.2011.19868.x](https://doi.org/10.1111/j.1365-2966.2011.19868.x)
- Jurcsik, J., Sódor, Á., Hajdu, G., et al. 2012b, *MNRAS*, 423, 993, doi: [10.1111/j.1365-2966.2012.20772.x](https://doi.org/10.1111/j.1365-2966.2012.20772.x)
- Jurcsik, J., Smitola, P., Hajdu, G., et al. 2017, *MNRAS*, 468, 1317, doi: [10.1093/mnras/stx382](https://doi.org/10.1093/mnras/stx382)
- Kalirai, J. S., Saul Davis, D., Richer, H. B., et al. 2009, *ApJ*, 705, 408, doi: [10.1088/0004-637X/705/1/408](https://doi.org/10.1088/0004-637X/705/1/408)
- Karczmarek, P., Pietrzyński, G., Górski, M., Gieren, W., & Bersier, D. 2017, *AJ*, 154, 263, doi: [10.3847/1538-3881/aa9574](https://doi.org/10.3847/1538-3881/aa9574)
- Kennedy, C. R., Stancliffe, R. J., Kuehn, C., et al. 2014, *ApJ*, 787, 6, doi: [10.1088/0004-637X/787/1/6](https://doi.org/10.1088/0004-637X/787/1/6)
- Kepler, S. O., Kleinman, S. J., Nitta, A., et al. 2007, *MNRAS*, 375, 1315, doi: [10.1111/j.1365-2966.2006.11388.x](https://doi.org/10.1111/j.1365-2966.2006.11388.x)
- Kervella, P., Gallenne, A., Remage Evans, N., et al. 2019a, *A&A*, 623, A116, doi: [10.1051/0004-6361/201834210](https://doi.org/10.1051/0004-6361/201834210)
- Kervella, P., Gallenne, A., Evans, N. R., et al. 2019b, *A&A*, 623, A117, doi: [10.1051/0004-6361/201834211](https://doi.org/10.1051/0004-6361/201834211)
- Kluyver, T., Ragan-Kelley, B., Pérez, F., et al. 2016, in *Positioning and Power in Academic Publishing: Players, Agents and Agendas*, ed. F. Loizides & B. Schmidt (Netherlands: IOS Press), 87–90. <https://eprints.soton.ac.uk/403913/>
- Kolenberg, K., Szabó, R., Kurtz, D. W., et al. 2010, *ApJL*, 713, L198, doi: [10.1088/2041-8205/713/2/L198](https://doi.org/10.1088/2041-8205/713/2/L198)
- Kovács, G. 2018, *A&A*, 614, L4, doi: [10.1051/0004-6361/201833181](https://doi.org/10.1051/0004-6361/201833181)
- Lam, S., Pitrou, A., & Seibert, S. 2015, 1–6, doi: [10.1145/2833157.2833162](https://doi.org/10.1145/2833157.2833162)
- Le Borgne, J. F., Poretti, E., Klotz, A., et al. 2014, *MNRAS*, 441, 1435, doi: [10.1093/mnras/stu671](https://doi.org/10.1093/mnras/stu671)
- Li, L. J., & Qian, S. B. 2014, *MNRAS*, 444, 600, doi: [10.1093/mnras/stu1344](https://doi.org/10.1093/mnras/stu1344)
- Li, L.-J., Qian, S.-B., Voloshina, I., et al. 2018a, *PASJ*, 70, 71, doi: [10.1093/pasj/psy061](https://doi.org/10.1093/pasj/psy061)
- Li, L. J., Qian, S. B., & Zhu, L. Y. 2018b, *ApJ*, 863, 151, doi: [10.3847/1538-4357/aad32f](https://doi.org/10.3847/1538-4357/aad32f)
- Liebert, J., Bergeron, P., Eisenstein, D., et al. 2004, *ApJL*, 606, L147, doi: [10.1086/421462](https://doi.org/10.1086/421462)
- Liška, J., Skarka, M., Mikulášek, Z., Zejda, M., & Chrástina, M. 2016a, *A&A*, 589, A94, doi: [10.1051/0004-6361/201525870](https://doi.org/10.1051/0004-6361/201525870)
- Liška, J., Skarka, M., Zejda, M., Mikulášek, Z., & de Villiers, S. N. 2016b, *MNRAS*, 459, 4360, doi: [10.1093/mnras/stw851](https://doi.org/10.1093/mnras/stw851)
- Martínez-Vázquez, C. E., Monelli, M., Gallart, C., et al. 2016, *MNRAS*, 461, L41, doi: [10.1093/mnras/slw093](https://doi.org/10.1093/mnras/slw093)
- Masuda, K., Kawahara, H., Latham, D. W., et al. 2019, *ApJL*, 881, L3, doi: [10.3847/2041-8213/ab321b](https://doi.org/10.3847/2041-8213/ab321b)
- Moe, M., & Di Stefano, R. 2017, *ApJS*, 230, 15, doi: [10.3847/1538-4365/aa6fb6](https://doi.org/10.3847/1538-4365/aa6fb6)
- Murphy, S. J., Bedding, T. R., & Shibahashi, H. 2016, *ApJL*, 827, L17, doi: [10.3847/2041-8205/827/1/L17](https://doi.org/10.3847/2041-8205/827/1/L17)
- Murphy, S. J., Moe, M., Kurtz, D. W., et al. 2018, *MNRAS*, 474, 4322, doi: [10.1093/mnras/stx3049](https://doi.org/10.1093/mnras/stx3049)

- Pedregosa, F., Varoquaux, G., Gramfort, A., et al. 2011, *Journal of Machine Learning Research*, 12, 2825
- Pietrzyński, G., Thompson, I. B., Gieren, W., et al. 2012, *Nature*, 484, 75, doi: [10.1038/nature10966](https://doi.org/10.1038/nature10966)
- Plachy, E., Molnár, L., Bódi, A., et al. 2019, *ApJS*, 244, 32, doi: [10.3847/1538-4365/ab4132](https://doi.org/10.3847/1538-4365/ab4132)
- Preston, G. W., Thompson, I. B., Sneden, C., Stachowski, G., & Shectman, S. A. 2006, *AJ*, 132, 1714, doi: [10.1086/507519](https://doi.org/10.1086/507519)
- Price-Whelan, A. M., Hogg, D. W., Rix, H.-W., et al. 2020, *ApJ*, 895, 2, doi: [10.3847/1538-4357/ab8acc](https://doi.org/10.3847/1538-4357/ab8acc)
- Prudil, Z., Skarka, M., Liška, J., Grebel, E. K., & Lee, C. U. 2019, *MNRAS*, 487, L1, doi: [10.1093/mnrasl/slz069](https://doi.org/10.1093/mnrasl/slz069)
- Prša, A., Guinan, E. F., Devinney, E. J., & Engle, S. G. 2008, *A&A*, 489, 1209, doi: [10.1051/0004-6361:200810486](https://doi.org/10.1051/0004-6361:200810486)
- Saha, A., Vivas, A. K., Olszewski, E. W., et al. 2019, *ApJ*, 874, 30, doi: [10.3847/1538-4357/ab07ba](https://doi.org/10.3847/1538-4357/ab07ba)
- Salinas, R., Hajdu, G., Prudil, Z., Howell, S., & Catelan, M. 2020, *Research Notes of the American Astronomical Society*, 4, 143, doi: [10.3847/2515-5172/abb022](https://doi.org/10.3847/2515-5172/abb022)
- Sandage, A. 1993, *AJ*, 106, 703, doi: [10.1086/116676](https://doi.org/10.1086/116676)
- Sesar, B., Hernitschek, N., Mitrović, S., et al. 2017, *AJ*, 153, 204, doi: [10.3847/1538-3881/aa661b](https://doi.org/10.3847/1538-3881/aa661b)
- Shibahashi, H. 2017, in *European Physical Journal Web of Conferences*, Vol. 152, European Physical Journal Web of Conferences, 03006, doi: [10.1051/epjconf/201715203006](https://doi.org/10.1051/epjconf/201715203006)
- Shibahashi, H., & Kurtz, D. W. 2012, *MNRAS*, 422, 738, doi: [10.1111/j.1365-2966.2012.20654.x](https://doi.org/10.1111/j.1365-2966.2012.20654.x)
- Shibahashi, H., Kurtz, D. W., & Murphy, S. J. 2015, *MNRAS*, 450, 3999, doi: [10.1093/mnras/stv875](https://doi.org/10.1093/mnras/stv875)
- Skarka, M., Liška, J., Dřevěný, R., et al. 2018, *MNRAS*, 474, 824, doi: [10.1093/mnras/stx2737](https://doi.org/10.1093/mnras/stx2737)
- Skarka, M., Prudil, Z., & Jurcsik, J. 2020, *MNRAS*, 494, 1237, doi: [10.1093/mnras/staa673](https://doi.org/10.1093/mnras/staa673)
- Smolec, R. 2016, in *37th Meeting of the Polish Astronomical Society*, ed. A. Róžańska & M. Bejger, Vol. 3, 22–25. <https://arxiv.org/abs/1603.01252>
- Smolec, R., Pietrzyński, G., Graczyk, D., et al. 2013, *MNRAS*, 428, 3034, doi: [10.1093/mnras/sts258](https://doi.org/10.1093/mnras/sts258)
- Sódor, Á., Skarka, M., Liška, J., & Bognár, Z. 2017, *MNRAS*, 465, L1, doi: [10.1093/mnrasl/slw194](https://doi.org/10.1093/mnrasl/slw194)
- Sódor, Á., Szeidl, B., & Jurcsik, J. 2007, *A&A*, 469, 1033, doi: [10.1051/0004-6361:20066886](https://doi.org/10.1051/0004-6361:20066886)
- Soszyński, I., Udalski, A., Szymański, M. K., et al. 2014, *AcA*, 64, 177. <https://arxiv.org/abs/1410.1542>
- . 2016, *AcA*, 66, 131. <https://arxiv.org/abs/1606.02727>
- Soszyński, I., Udalski, A., Wrona, M., et al. 2019, *AcA*, 69, 321, doi: [10.32023/0001-5237/69.4.2](https://doi.org/10.32023/0001-5237/69.4.2)
- Stancliffe, R. J., Kennedy, C. R., Lau, H. H. B., & Beers, T. C. 2013, *MNRAS*, 435, 698, doi: [10.1093/mnras/stt1329](https://doi.org/10.1093/mnras/stt1329)
- Sterken, C. 2005, in *Astronomical Society of the Pacific Conference Series*, Vol. 335, *The Light-Time Effect in Astrophysics: Causes and cures of the O-C diagram*, ed. C. Sterken, 3
- Szeidl, B., Hurta, Z., Jurcsik, J., Clement, C., & Lovas, M. 2011, *MNRAS*, 411, 1744, doi: [10.1111/j.1365-2966.2010.17815.x](https://doi.org/10.1111/j.1365-2966.2010.17815.x)
- Torreálba, G., Catelan, M., Drake, A. J., et al. 2015, *MNRAS*, 446, 2251, doi: [10.1093/mnras/stu2274](https://doi.org/10.1093/mnras/stu2274)
- Troup, N. W., Nidever, D. L., De Lee, N., et al. 2016, *AJ*, 151, 85, doi: [10.3847/0004-6256/151/3/85](https://doi.org/10.3847/0004-6256/151/3/85)
- Udalski, A., Szymański, M. K., & Szymański, G. 2015a, *AcA*, 65, 1. <https://arxiv.org/abs/1504.05966>
- Udalski, A., Soszyński, I., Szymański, M. K., et al. 2015b, *AcA*, 65, 341. <https://arxiv.org/abs/1601.01683>
- Virtanen, P., Gommers, R., Oliphant, T. E., et al. 2020, *Nature Methods*, 17, 261, doi: [10.1038/s41592-019-0686-2](https://doi.org/10.1038/s41592-019-0686-2)
- Vivas, A. K., Walker, A. R., Martínez-Vázquez, C. E., et al. 2020, *MNRAS*, 492, 1061, doi: [10.1093/mnras/stz3393](https://doi.org/10.1093/mnras/stz3393)
- Vos, J., Bobrick, A., & Vučković, M. 2020, *A&A*, 641, A163, doi: [10.1051/0004-6361/201937195](https://doi.org/10.1051/0004-6361/201937195)
- Wade, R. A., Donley, J., Fried, R., White, R. E., & Saha, A. 1999, *AJ*, 118, 2442, doi: [10.1086/301109](https://doi.org/10.1086/301109)
- Zhang, Z. H., Homeier, D., Pinfield, D. J., et al. 2017, *MNRAS*, 468, 261, doi: [10.1093/mnras/stx350](https://doi.org/10.1093/mnras/stx350)